



First surface measurement of variation of Cloud Condensation Nuclei (CCN) concentration over the Pristine Himalayan region of Garhwal, Uttarakhand, India

Alok Sagar Gautam^a, S.N. Tripathi^{b,*}, Abhishek Joshi^{c,*}, Anil Kumar Mandariya^b, Karan Singh^c, Gaurav Mishra^d, Sanjeev Kumar^a, R.C. Ramola^c

^a Department of Physics, Hemvati Nandan Bahuguna Garhwal University Srinagar Uttarakhand, India

^b Department of Civil Engineering, Indian Institute of Technology, Kanpur, India

^c Department of Physics, Hemvati Nandan Bahuguna Garhwal University, Badshahi Thaul Campus, Tehri Garhwal, Uttarakhand, India

^d Nuclear Engineering and Technology Programme, Department of Mechanical Engineering, IIT, Kanpur, India

HIGHLIGHTS

- Time series of CCN at four different levels of supersaturation (Supersaturation: 0.2, 0.5, 0.8, and 1.0%), and its role in the macroscopic cloud formation mechanism over the high-altitude region.
- Study of seasonal, diurnal, and temporal variation of CCN over the Himalayan regions and comparisons with different altitude sites, geographic and climatic conditions of India.
- Observations provided the average CCN concentration $1411.3 \pm 1110.1 \text{ cm}^{-3}$, $1645.7 \pm 690.62 \text{ cm}^{-3}$, $1712.3 \pm 862.8 \text{ cm}^{-3}$, and $2514.7 \pm 2166.4 \text{ cm}^{-3}$ for Monsoon, Post- Monsoon, Winter and Pre-monsoon Seasons respectively.
- Analysis of local meteorological conditions impact on the formation of high-altitude cloud, and complexity of local weather phenomenon.
- Use of transport models to analyze and characterize the possible sources of the pollutant for rural areas with relatively low urbanization and industrialization activities and role transported pollutants from the urban (highly polluted and populated) regions on the modification of local meteorology of the Garhwal Himalayan regions.

ARTICLE INFO

Keywords:

CCN
Aerosols
Garhwal region
Air-mass back trajectory
CWT

ABSTRACT

A Droplet Measurement Technology (DMT) Cloud Condensation Nuclei Counter (CCNC) was deployed to measure cloud condensation nuclei (CCN) for the first time in the pristine Himalayan region at Himalayan Clouds Observatory (HCO), Swami Ram Tirtha (SRT) Campus (30°34' N, 78°41' E, 1706 m AMSL), Hemvati Nandan Bahuguna (HNB) Garhwal University, Badshahithaul, Tehri Garhwal, Uttarakhand, India. The CCN concentration (N_{CCN}) was observed at four supersaturation levels (SS: 0.2, 0.5, 0.8, and 1.0%). In this study, we reported CCN concentration at 0.5% SS in different weather conditions from Aug 01, 2018 to Jun 30, 2019. During this observation period, the monthly averaged value of CCN concentration ranged between $1098.3 \pm 448.9 \text{ cm}^{-3}$ (mean \pm SD) and $3842.9 \pm 2512.9 \text{ cm}^{-3}$. It covers a significantly wide range of daily averaged concentrations from the minimum concentration of 43.84 cm^{-3} (during heavy wet scavenging due to snowfall) to maximum concentration of 17000 cm^{-3} (during the events of a forest fire) at the observation site. The highest CCN concentration is observed at the time of sunrise (~07:00 a.m.) and after the sunset (~07:00 p.m.) for the diurnal variation of monsoon, post-monsoon, and winter season. Pre-monsoon season shows peak values at 10:00 a.m. and at 07:00 p.m. with higher concentrations at night hours. The possible reasons for maximum concentration in morning and evening time could be upliftment and settlement of CCN because of the convection process, anthropogenic emission, vehicular emission, and biomass burning in the residential area and valley region adjacent to HCO, Badshahithaul. The highest CCN concentration ($3842.9 \pm 2513 \text{ cm}^{-3}$) values of the whole observation period were observed in May 2019. It was significantly affected by the heavy fire activities over the

* Corresponding author.

** Corresponding author.

E-mail addresses: snt@iit.ac.in (S.N. Tripathi), abhijmuki28@gmail.com (A. Joshi).

Uttarakhand and nearby IGP regions. Diurnal variation of CCN concentration during the HFAD shows higher values in the night time differing from the diurnal pattern of CCN for other months of the observation period. The long-range transport of air mass could also contribute to the high CCN concentration values, as found through the five-day air mass backward trajectory analysis. The lowest value of CCN concentration corresponds to the heavy rains and snowfall days, possibly caused by extensive wet scavenging. Cluster analysis of the air mass trajectories used for the allocation and classification of the possible sources of pollutants reaching the observation site. The highest fraction of CCN concentration (more than 2000 cm^{-3}) corresponds to the air mass from the arid and semi-arid regions of Asian countries. Large air mass fraction ($\sim 40\text{--}60\%$) with moderate CCN concentration was received from northwestern IGP region and foothills of central Himalaya.

1. Introduction

Condensation Nuclei (CN) that activate and become Cloud Condensation Nuclei (CCN) play an essential role in the earth's climate and the hydrological cycle through their direct and indirect effects (Haywood, 2016). CN produced by anthropogenic as well as natural sources, can directly influence climate by reflecting or absorbing the solar radiation (Ramanathan et al., 2001). CCN can activate and grow into fog or cloud droplets in the presence of supersaturation (Che et al., 2016), which influences cloud microphysical properties by seeding clouds, radiative properties such as cloud albedo and cloud lifetime (IPCC, 2014), and thus rainfall patterns (Rosenfeld et al., 2014; Sarangi et al., 2014; Twomey, 1977; Pruppacher and Klett, 1997; Ramanathan et al., 2001).

The size spectrum of the atmospheric aerosol ranges from nanometer to a few micro-meter (Tang et al., 2019). These particles could be

produced in the atmosphere through two processes; the first one is direct emissions to the atmosphere. The other is the oxidation of its precursor gases (e.g., Sulphur dioxide, Nitrogen dioxide, and Volatile organic gases (VOCs)). Particles formed by these two processes are known as Primary and Secondary particles, respectively (Finlayson-Pitts, 1997; Seinfeld et al., 1998). The product of the oxidation process could nucleate to form new particles under higher solar radiation and high temperature (Gautam et al., 2017; Kanawade et al., 2014; Roy et al., 2017) or condense on pre-existing particles. Freshly emitted soot particles with low hygroscopic nature became more CCN active by oxidation and condensation of co-emitted hydrophilic vapors. (Khalizov et al., 2013).

Features such as cloud droplet number concentration (CDNC), cloud dynamics, and structure are determined by CCN number concentration. Several previous studies found that the formation of cloud droplets can

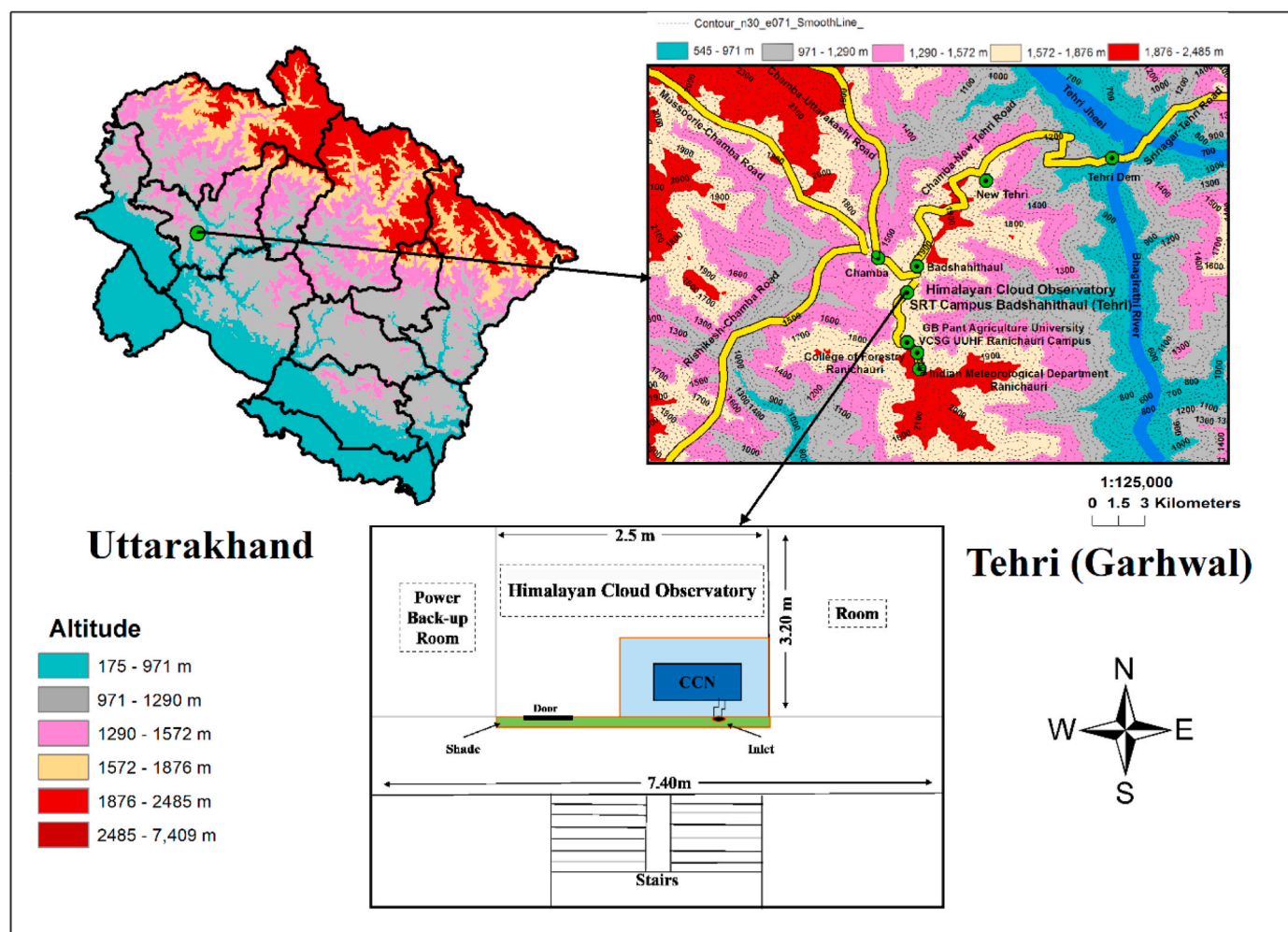


Fig. 1. Topographic map of observation site and surroundings with the schematic diagram of the Himalayan Cloud Observatory (HCO), Swami Ram Tirth campus, Tehri Garhwal, Uttarakhand (India).

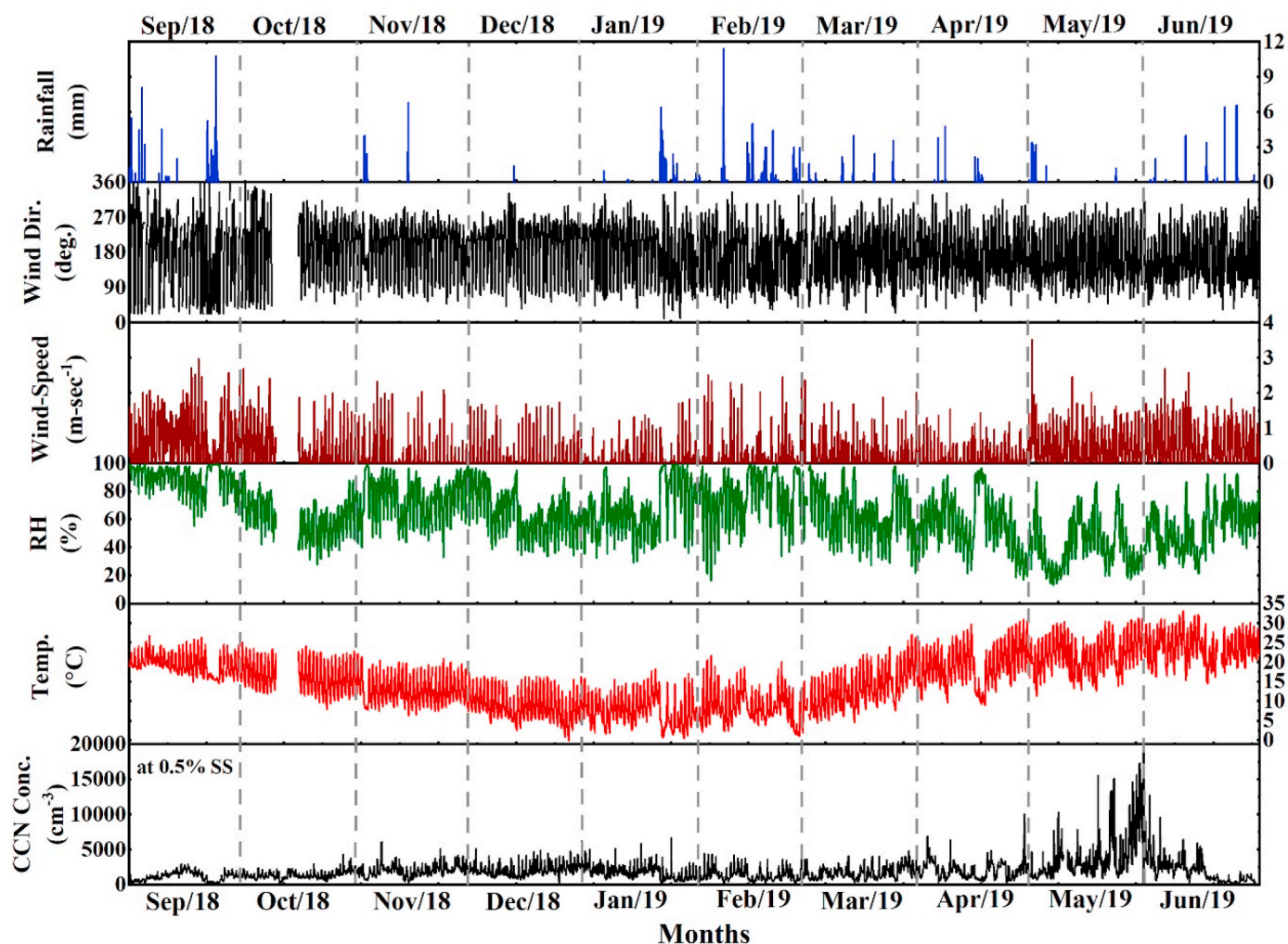


Fig. 2. Temporal variation of hourly averaged meteorological parameters with CCN concentration at 0.5% SS observed at HCO, SRT Campus, HNB Garhwal University, Badshahithaul; Sep 01, 2018 to Jun 30, 2019. (Meteorological data between Oct 10 to Oct 15, 2018 is not available due to the instrumental error).

be governed by the presence of CCN and updraft velocity, globally (Bougiatioti et al., 2017; Reutter et al., 2009; Rosenfeld et al., 2014). Particle size distribution and their chemical composition are deciding factors for the ability of the aerosol particle to act as CCN (Bougiatioti et al., 2017). Previous studies showed that the variability in aerosol chemical composition is less significant and has less contribution than the variability in aerosol size distribution (Crosbie et al., 2015; Dusek et al., 2006; Ervens et al., 2007). Organic aerosols contribute to the significant fraction of CCN relevant aerosol on a global scale. Several studies (Almeida et al., 2014; Bhattu and Tripathi, 2015; Hudson, 2007; Zhang et al., 2007) suggested the importance of the size-resolved chemical composition, bulk composition, and state of mixing of the aerosol particles. Inter-seasonal size-resolved CCN variability shows lower participation of CCN-inactive particles at higher supersaturation (Bhattu and Tripathi, 2014).

Indo-Gangetic Plain (IGP) is one of the most highly polluted and populated regions of the world and has a variety of sources of anthropogenic aerosols (Dey and Di Girolamo, 2010; Gautam et al., 2011; Kanaawade et al., 2014; Kedia et al., 2014; Panicker et al., 2019; Rajput et al., 2016; Srivastava et al., 2011). The thick layer of haze formed due to the anthropogenic aerosol is called Atmospheric Brown Cloud (ABC) and can affect cloud-radiation interaction and precipitation activities over IGP and adjacent Himalayan regions (Bonasoni et al., 2010; Lüthi et al., 2014; Ramanathan et al., 2005). Mixing of aerosols during long-range transportation affects the chemical properties of aerosol

(Wang et al., 2005). Aged dust and aerosols generated from biomass burning and anthropogenic activities could contribute considerably to CCN concentration and CCN activation (Roy et al., 2017). Aerosols produced from biomass burning in the nearby fire-impacted sectors could also increase the CCN concentration (Ram et al., 2014). Recent studies (Bhattu and Tripathi, 2014; Patidar et al., 2012; Ram et al., 2014) investigated the submicron aerosol's ability to act CCN at various degrees of supersaturation over an urban atmosphere of Kanpur situated at IGP. Besides some other studies (Dumka et al., 2015; Gogoi et al., 2015) examined the effect of anthropogenic aerosols transported from IGP regions on the CCN number concentration at Nainital, Kumaun region of Uttarakhand in western Himalaya. However, no study has yet reported temporal variation of CCN number concentration over the elevated Himalayan site. To the extent of our knowledge, the Garhwal region of the western Himalaya, Uttarakhand, is still unexplored. The current study presents the first long-term CCN observations on seasonal scales observed at the Himalayan Clouds Observatory (HCO). The HCO was established to take real-time ground-based observations for the study of CCN and other meteorological parameters (such as; Temperature, Humidity, Wind Speed & Direction, Solar Radiation, and Rainfall) on the western part of Garhwal Himalayan region of Uttarakhand. This study will be helpful in understanding the complex mechanism of cloud burst and weather extremities over the sensitive Himalayan region under different-weather conditions (Clear, Cloudy, Rainy, and Snowfall).

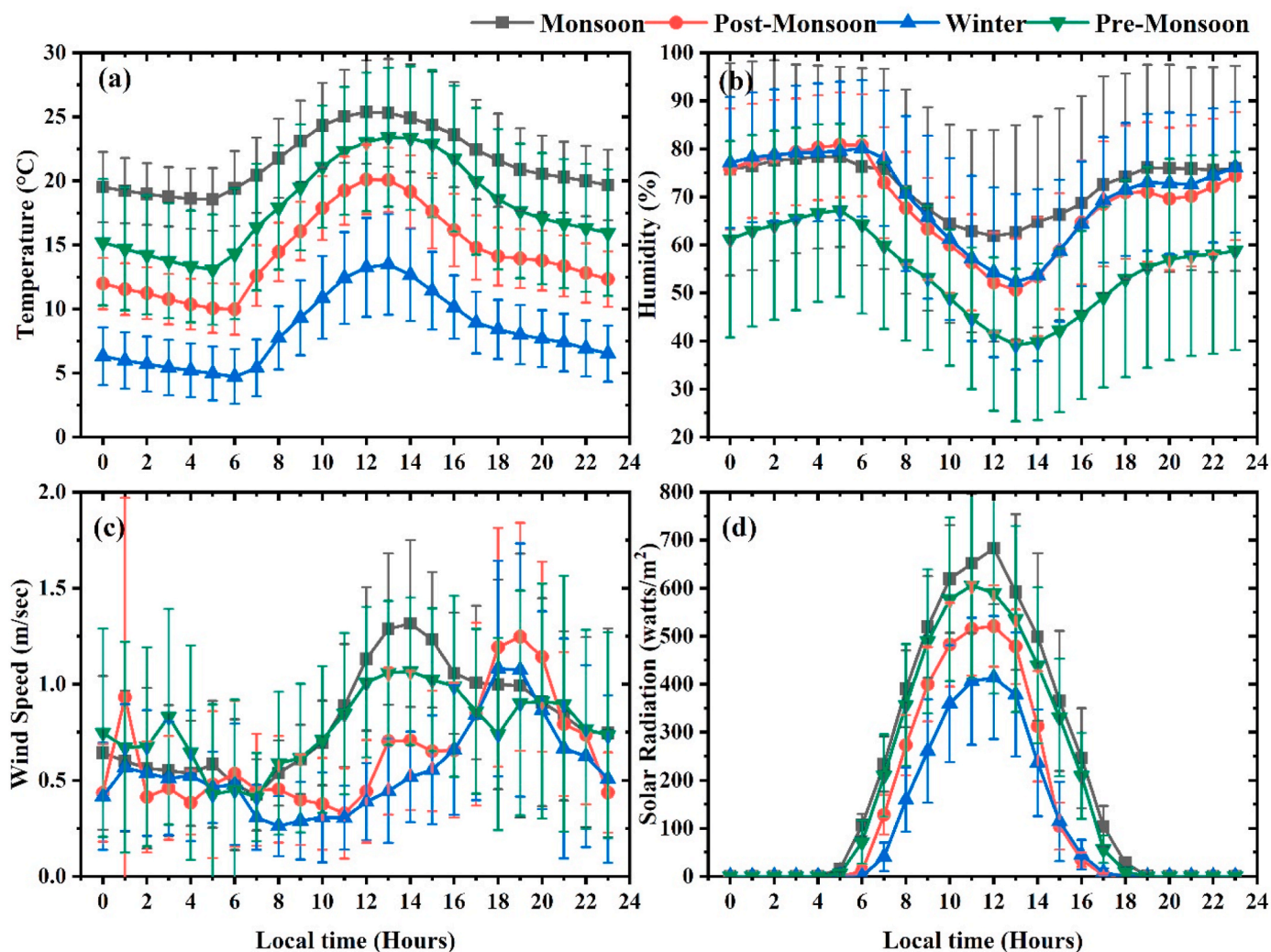


Fig. 3. Diurnal variation of meteorological parameters at Observation site (a) Temperature (b) Relative Humidity (c) Wind speed and (d) Solar radiation for Monsoon-M (Sep 2018, Jun 2019); Post Monsoon-PoM (Oct – Nov 2019); Winter-W (Dec 2018, Jan – Feb 2019) and Pre-Monsoon-PrM (Mar – May 2019) season.

2. Observation site and instrumentation

Tehri Garhwal is one of the largest districts in the hill state of Uttarakhand with a surface area of 3642 km² and a population density of 170 inhabitants per km² (CENSUS, 2011). This region has a sub-temperate to temperate climate, which remains consistently pleasant throughout the year. Major crop types in this region are Rice, Wheat, Mandua, and Oilseeds. It is rich in fruits and vegetable production. Major mineral types found in this region are magnesite, dolomite, limestone, tin, phosphate, and marble. Subtropical forest species grow in the outer range of low hills to abundant alpine flowers in the north containing a wide variety of trees such as Pine, Oak, Conifers, Sal, Deodar, Yew, and Cypress (DCMSME, 2016).

Fig. 1 represents the topographic view of the geographical area around the SRT campus, Badshahithaul, and schematic diagram of the observation laboratory. The elevation map is plotted using the United States Geographical Survey (USGS) earth explorer digital elevation models (DEM) data (Usery et al., 2009) and digitized on QGIS (an Open Source Geographic Information System tool). The Observation site is regarded as the Himalayan Cloud Observatory (HCO). It is located on the slope of the lesser Himalayan mountain range surrounded by the dense forest of Alpine, Oak, and Deodar trees. The observation site is situated in the Department of Physics, Hemvati Nandan Bahuguna (HNB) Garhwal University, SRT Campus, Badshahithaul (30.33° N and 78.40°

E), Tehri Garhwal, Uttarakhand at an altitude of 1706 m above mean sea level (AMSL).

The HCO is situated in the outer regions of New Tehri and Chamba cities (8 km and 3 km away from the city center to the North East and Northwest, respectively). College of Forestry, Veer Chandra Singh Garhwali University of Horticulture and Forestry, Ranichauri and Indian Meteorological Department (IMD), Ranichauri are at the distance of ~3 km in the South direction to the SRT campus, Badshahithaul at an altitude ranging between 1600 and 2200 m (AMSL) (Upadhyay et al., 2015). The local residential area is within 300 m of HCO and a small college canteen in 100 m range. The national highway (NH-34) passes with moderate traffic on the other side of the hill in the West direction. The site has no major industrial activities in a radius of 10 km, but the Tehri Dam Hydro Project is within the range of 25 km.

A continuous-flow streamwise thermal gradient single column CCN counter (CCNC) is used to measure the CCN number concentration (Lance et al., 2006; Roberts and Nenes, 2005; Rose et al., 2008) for the entire sampling period of Aug 01, 2018 to Jun 30, 2019. It operates on the principle that diffusion of heat in the air is slower than the diffusion of the water vapor and based on the design of Robert and Nenes. The operation of CCNC is described in detail elsewhere (Rose et al., 2008). CCNC was calibrated for various degrees of supersaturation before measurements at HCO laboratory using (NH₄)₂SO₄ aerosols following the standard procedure reported elsewhere (Figure S1) (Patidar et al.,

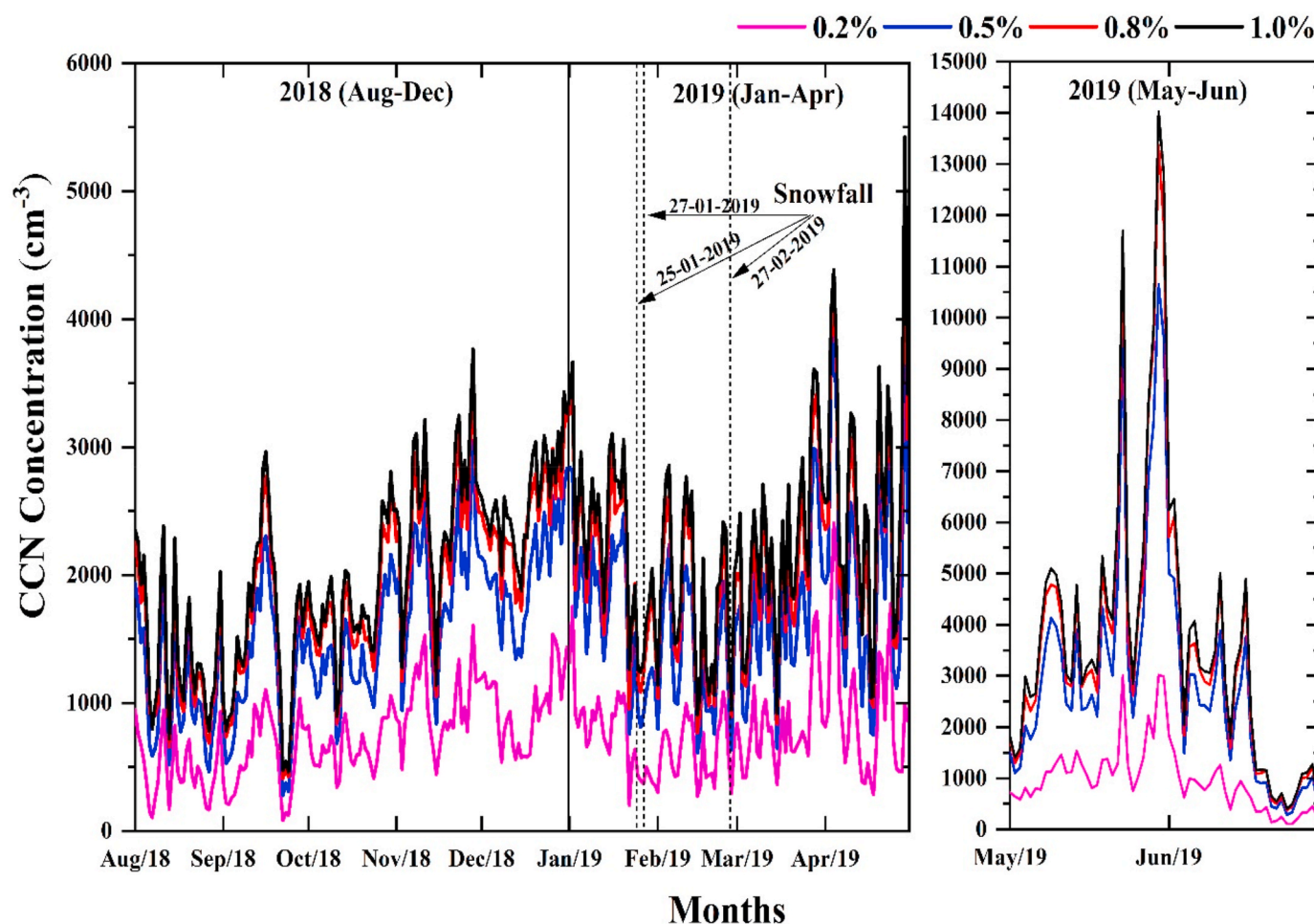


Fig. 4. Temporal variation of daily averaged CCN concentration at observed Super saturations (0.2, 0.5, 0.8 and 1.0%) for the entire period of observations.

2012; Rose et al., 2008). An inbuilt pump sucks ambient air at a constant flow rate ($500 \text{ cm}^3 \text{ min}^{-1}$) inside the CCNC chamber, where activated particle converted eventually into cloud droplets by condensation at a particular SS (ranges between 0.07 and 2%). Activated particle within the sizing range of $0.75 \text{ }\mu\text{m}$ – $1.0 \text{ }\mu\text{m}$ counted with the help of an Optical Particle Counter (OPC). CCN measurements were made for 5 min at each of the four SS (0.2, 0.5, 0.8, and 1.0%). The first 2 min of data out of the 5-min data for each SS were discarded due to unstable thermal conditions inside the column (Dumka et al., 2015). The rest of the data is averaged hourly, monthly, and seasonally for the further analysis process.

Meteorological parameters (temperature, wind speed and direction, humidity, rain, and solar radiation) are continuously measured with the help of an Automatic Weather Station (AWS) installed at HCO, Badshahithaul, for the observation period (Sep 01, 2018, to Jun 30, 2019). The month of Aug 2018 is not included in this study due to unavailability of the meteorological data during this month. The meteorological parameters were recorded at the 1-min interval and analyzed using the hourly and daily average values during the observation. Wind speed (range and accuracy: 0.5 – 67 m/s , 0.5 m/s) and direction (full 360 , ± 0.3 – 0.5) and solar radiation flux density (0 – 2000 W/m^2 , $\pm 5\%$) were measured with the help of Anemometer and Pyranometer, respectively. High accuracy temperature (-40 to $+123.8 \text{ }^\circ\text{C}$, $\pm 0.1 \text{ }^\circ\text{C}$) and relative humidity (0 – 100% , $\pm 2\%$) sensors are used to measure the temperature, and relative humidity, whereas rainfall is measured with the help of a digital rain gauge (100 mm/h , $\pm 5\%$). Details of the instruments are available at <http://vhydromet.com/index.php>.

A Hybrid Single-Particle Lagrangian Integrated Trajectory

(HYSPLIT4) model (Stein et al., 2015) was used to calculate the five days back trajectory (BT) of air mass to analyze the influence of long-range transported air masses, arriving at 500 m above ground level (AGL). The input meteorological data were acquired from NOAA's Global Data Assimilation System (GDAS, $1^\circ \times 1^\circ$). Seasonal BT was plotted for different seasons; monsoon (Aug–Sep 2018, Jun 2019), post-monsoon (Oct–Nov 2018), winter (Dec 2018, Jan–Feb 2019), and pre-monsoon (Mar–May 2019) to investigate the possible sources of CCN inclusive air mass arriving at the observation site (HCO). Further, all trajectories were grouped by multivariate statistical tools, i.e., cluster analysis to classify the sources of pollutants. The obtained trajectories have been clustered based on the similarities of the spatial distribution using HYSPLIT software. The complete process is described in the user guide of the software (Draxler et al., 2014). On the basis of the change in the total spatial variance, the optimum numbers of clusters considered for each season and mean BTs for each cluster of all seasons were calculated.

The contribution of sources from different regions to the CCN concentration is computed by Concentration Weighted Trajectories (CWT) analysis using Trajstat (V-1.4.4). Each grid cell is assigned a weighted concentration using the following equation (Equation. 1) in the CWT method (Hsu et al., 2003; Seibert et al., 1994):

$$C_{ij} = \frac{1}{\sum_{l=1}^M \tau_{ijl}} \sum_{l=1}^M C_l \tau_{ijl} \quad (1)$$

Where C_{ij} is the average weighted concentration in the ij th cell, l is the index of the trajectory, M is the total number of trajectories, C_l is the concentration observed on the arrival of trajectory l , and τ_{ijl} is the time

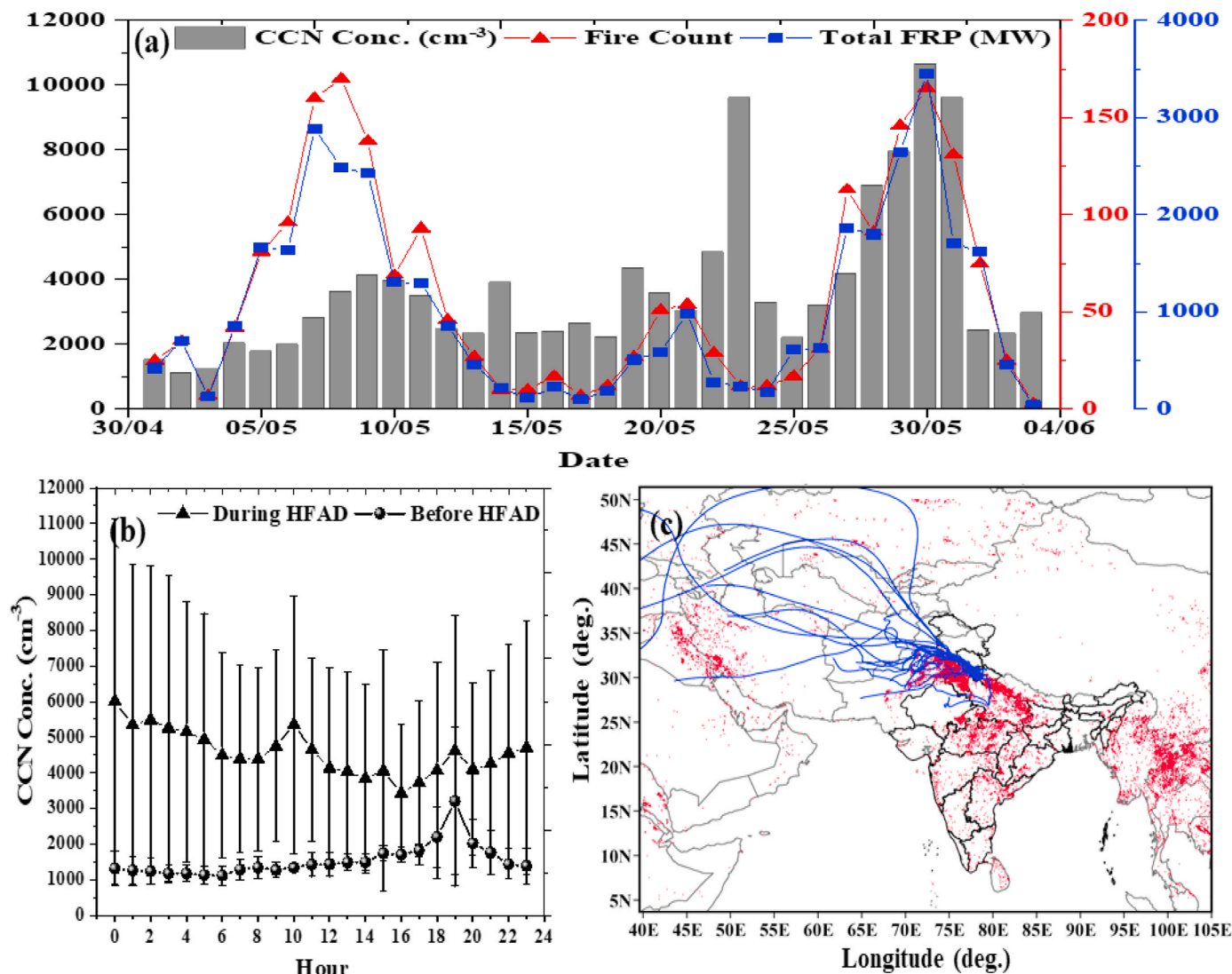


Fig. 5. Variation of CCN concentration with MODIS retracted fire events between 01 May to Jun 03, 2019 (a) temporal variation of CCN concentration with fire count and daily total fire radiative power (May 19), (b) Diurnal variation of CCN concentration for before and after High fire activity days (HFAD), (c) air mass back trajectory arriving at 500 mAGL, with MODIS fire count showing the hot spots of fire during HFAD.

spent in the ij th cell by trajectory l .

3. Meteorological conditions

The background meteorological conditions are represented (Fig. 2) as time series of the hourly average of meteorological parameters (temperature, relative humidity, wind speed, wind direction, and rainfall) along with the CCN concentration at 0.5% SS. The hourly average ambient temperature varied from -0.7 during Jan 2019 to 33.2 °C in Jun 2019. The ambient relative humidity was observed minimum during Oct 2018 ($\sim 30\%$) and maximum during Sep 2018 and Jun 2019 ($>90\%$). The site was observed to have higher relative humidity during the monsoon season as compared to winter fog conditions. Jan 2019 and Feb 2019 months received snowfall events along with a few events of rainfall. Maximum solar radiation received up to 820 Wm^{-2} in May 2019. Sep 2018 receives the most substantial amount of rain throughout the month. Diurnal variation of observed meteorological parameters for various seasons; monsoon (M) season (JS; Sep 2018, Jun 2019), post-monsoon (PoM) season (ON; Oct–Nov 2018), winter (W) season (DJF; Dec 2018, Jan–Feb 2019), and pre-monsoon (PrM) season (MAM; Mar–May 2019) have illustrated in Fig. 3. The classification of various seasons has been done as mentioned by (Upadhyay et al., 2015). Aug

2018 is not included in the M season here due to the unavailability of meteorological data; although, it is included in the M season for CCN data. Also, only Jun 2019 was included in M season for solar radiation data, while other seasons contain the same months as mentioned in the earlier text in the present study. The diurnal variation of M reported the highest temperature and relative humidity throughout the day. Higher wind activities have been observed mainly during evening time (18:00–20:00 h) in the PoM and W seasons. However, the site was affected by dominant southwesterly winds for almost all seasons of the observation period, influenced by upslope valley wind patterns due to the topography of the region. This kind of wind pattern possibly indicates air masses transportation from arid and semi-arid regions of northwestern IGP regions of India, Pakistan, and western parts of Asia (Devi et al., 2011; Dumka et al., 2015).

4. Results and discussion

4.1. Temporal variation of CCN

Temporal variation of daily averaged CCN number concentrations at four different SS for the study period have illustrated in Fig. 4. Average value of daily CCN concentration for complete period is $1843.7 \pm$

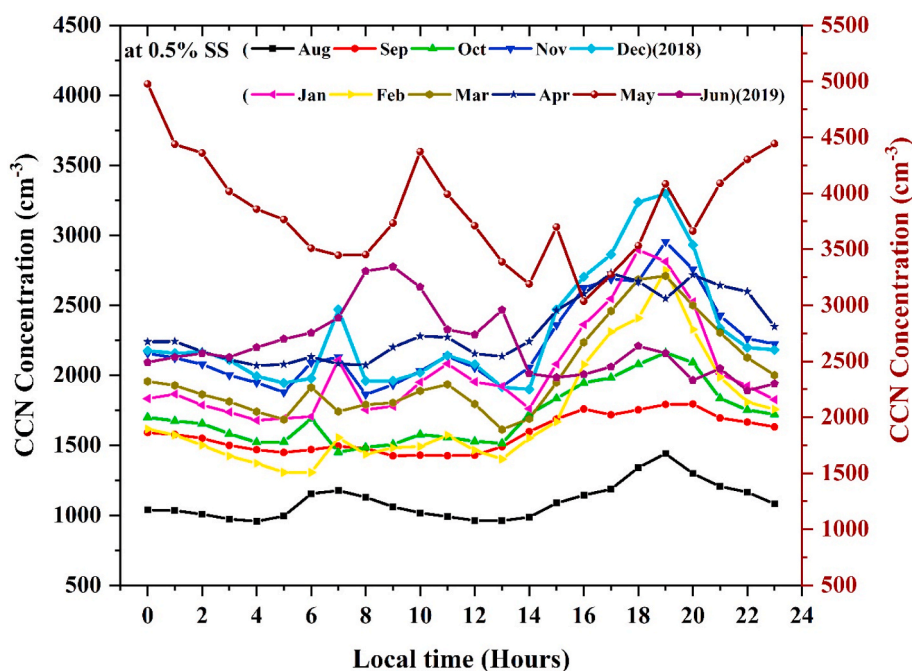


Fig. 6. Diurnal variation of CCN for each months of the observation period at 0.5% SS (Aug 2018-Jun 2019). (Secondary, Y-axis on the right side is for the CCN concentration of May 2019 only).

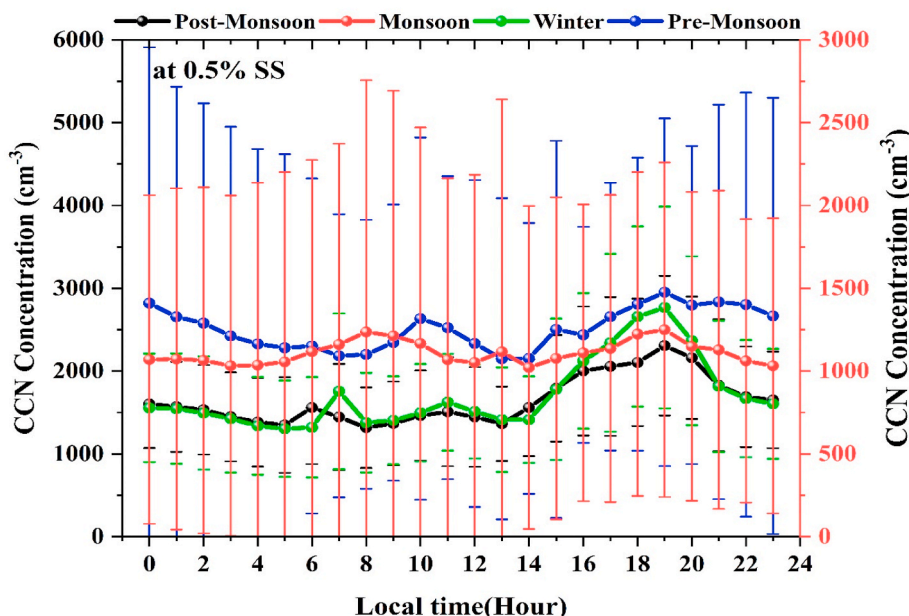


Fig. 7. Diurnal variation of CCN concentration of M(Aug – Sep 2018, Jun 2019); PoM(Oct – Nov 2019); W(Dec 2018, Jan – Feb 2019) and PrM(Mar – May 2019) season at 0.5% SS (Secondary Y-axis on the right side is for the CCN concentration of monsoon season).

1219.5 cm^{-3} (mean \pm SD) with 10649.9 cm^{-3} and 277.4 cm^{-3} maximum and minimum value respectively at 0.5% SS. The temporal variation consists of several peaks associated with a variety of events such as forest fires, long-range transportation, and influence by nearby local emission sources. In contrast, the downward trend showed an association with atmospheric events like wet scavenging via rain and snowfall. The CCN concentration is appeared to gradually increase with increment in SS (Dumka et al., 2015; Jefferson, 2010). The lowest CCN concentration, 277.4 cm^{-3} (0.5% SS), was recorded on Sep 22, 2018 due to heavy rainfall events. Also, HCO experienced few light snowfall (Approx. 5 cm) events on Jan 22, 2018 (757.3 cm^{-3}), Jan 25, 2019

(931.7 cm^{-3}), and Feb 27, 2019 (636.3 cm^{-3}), which were associated with lower CCN concentration mainly due to accretion process of supercooled cloud droplets (Borys et al., 1996). The observation site is surrounded by dense forest, which results in the massive forest fire in the last week of May to the first week of Jun every year; however, this year 2019, the heavy forest fire events occurred between May 04 to Jun 03, 2019. The highest CCN Concentration, 10649.9 cm^{-3} (0.5% SS), was reported on May 30, 2019, possibly attributed by the significant contribution of large forest fire emissions (Sánchez et al., 2017; Singla et al., 2019). MODIS Collection 6 data obtained from Fire Information for Resource Management System (FIRMS) was used to quantify the

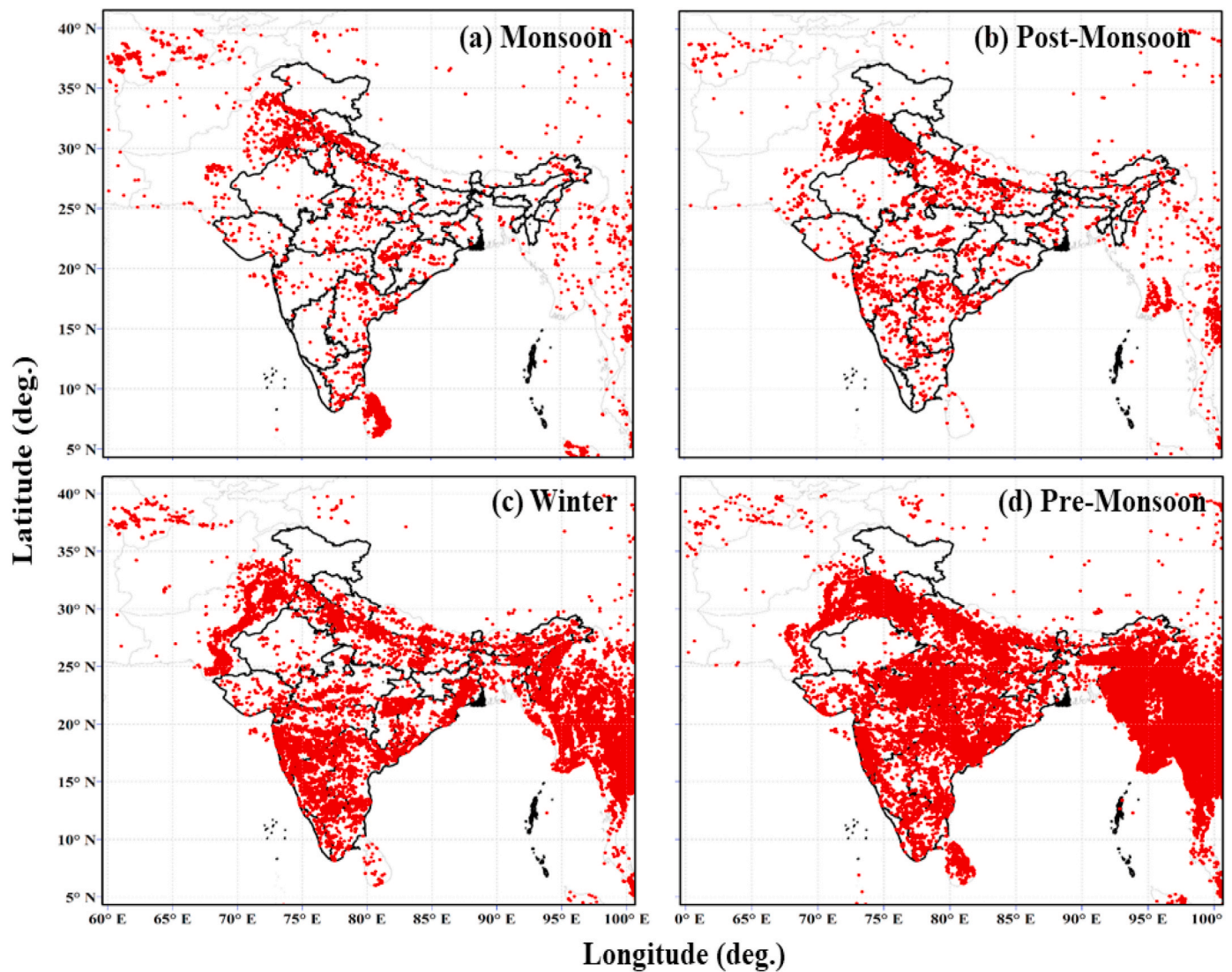


Fig. 8. Active fire counts for (a) M(Aug – Sep 2018, Jun 2019); (b) PoM(Oct – Nov 2018); (c) W(Dec 2018, Jan – Feb 2019) and (d) PrM(Mar – May 2019) season over the Indian subcontinent derived from the MODIS dataset.

burning activities in India and nearby countries in May 2019. The active fire data was taken for the rectangular grid (between latitude - 28°43' N to 31°27' N and longitude - 77°34' E to 81°02' E) over Uttarakhand (DCMSME, 2016). Fig. 5a shows the temporal variation of daily total fire count and total fire radiative power (FRP) with the CCN concentration. It is observed that high fire count corresponds to the high value of CCN concentration. It shows two prominent peaks during this month, first on May 08, 2019 and the other on May 30, 2019. The increased fire activities were recorded around May 20, which possibly results in a significant increased CCN concentration, as observed on the subsequent days (peak on May 23, 2019). Fig. 5b shows the diurnal variation of CCN concentration for the period between May 01 to Jun 03, 2019. This period is categorized into two parts; before high fire activity period (HFAD) May 01 – May 03) and during high fire activity (May 04 – Jun 03). This classification is based on the method mentioned by (Yarragunta et al., 2020). According to this method, if three days running mean of MODIS fire count data exceeds the median of whole fire count, then it is considered as the HFAD (Bhardwaj et al., 2018; Kumar et al., 2011). Before HFAD, the diurnal pattern is almost the same for the whole day, with a distinct peak in the evening (17:00 h). During HFAD considerably high concentration is observed in the night hours with few peaks in the day time. Apart from the local activities, the long-range transport of air

mass also plays an important role in the CCN concentration. Fig. 5c shows air mass arriving from the area of high fire activities with the hotspots over the western part of the IGP regions. The impact of long-range transport of different types of pollutants on the CCN concentration is explained in section 4.4.

4.2. Diurnal variation of CCN

The diurnal variation of CCN at 0.5% SS for all individual months showed in Fig. 6. CCN showed a dynamic diurnal variation for different months of the observation period. The difference between the highest and lowest value of N_{CCN} was minimum (416.6) for Sep 2018 and maximum (1939) for May 2019. However, CCN showed its maximum ($3846.5 \pm 472.9 \text{ cm}^{-3}$) and minimum ($1099.4 \pm 129.0 \text{ cm}^{-3}$) value in the average diurnal variation during May 2019 and Aug 2018, respectively. The lowest values observed in Aug 2018 were potentially due to the wet scavenging of aerosol particles by high precipitation that suppresses the concentration of CCN particles (Garrett et al., 2006). Similarly, a good association of lower diurnal values with wet scavenging through raindrops was observed for Sep 2018. While on the other hand, the variation range of N_{CCN} is maximum for May 2019 (between 3036 and 4975 cm^{-3}) due to the heavy aerosol loading by the events of forest

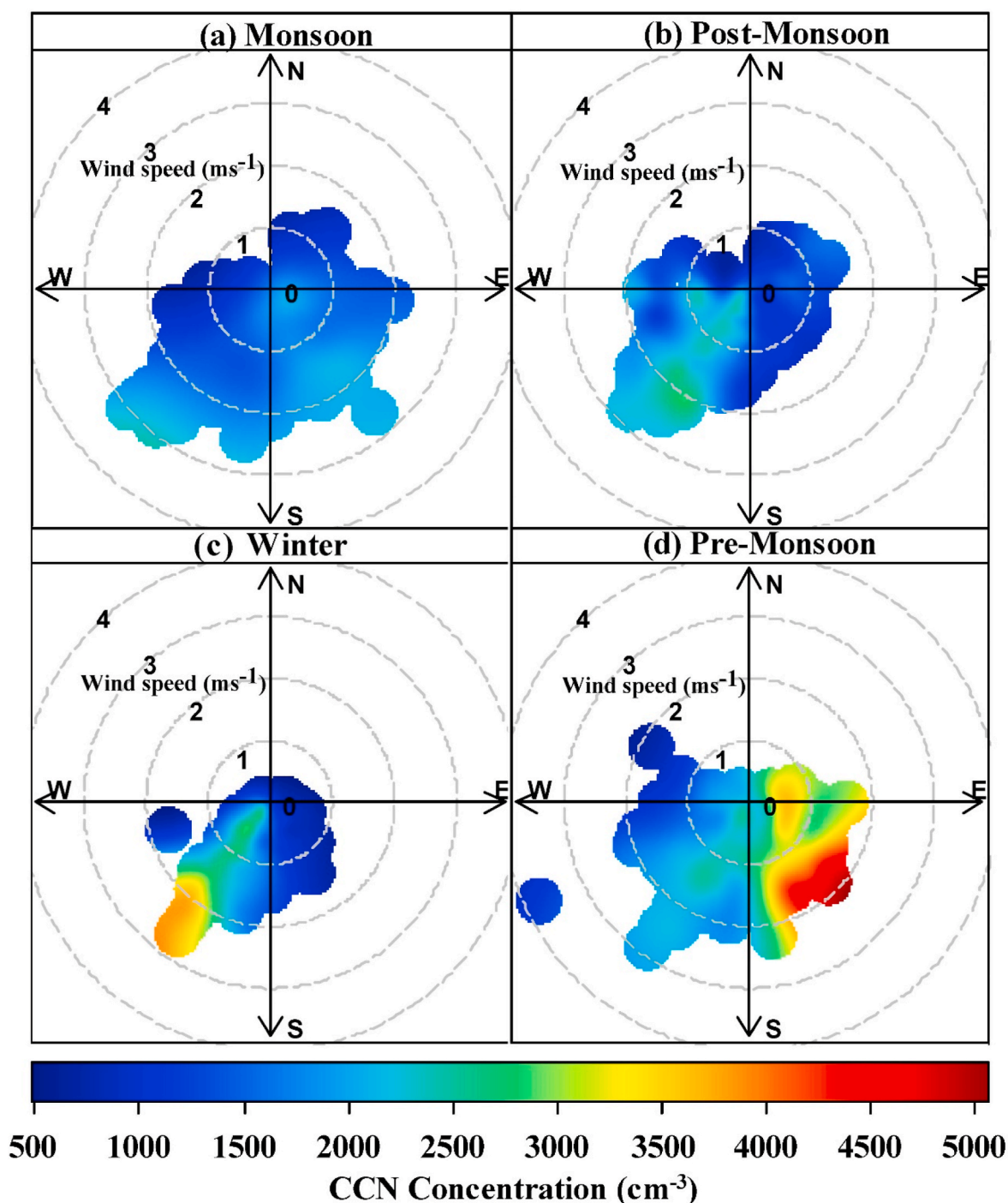


Fig. 9. Polar plots for wind dependency of CCN concentration (cm^{-3}) at 0.5% SS for (a) M(Sep 2018, Jun 2019); (b) PoM(Oct – Nov 2018); (c) W(Dec 2018, Jan – Feb 2019) and (d) PrM(Mar – May 2019) season.

fire and long-range transport of aerosol. The high fire activities significantly influence the diurnal pattern of the concentration for May and Jun 2019, explained in section 4.1 of this study. Shallow boundary layer height in the night hours brings the pollutants produced from biomass burning close to the ground surface (Li et al., 2015; Miao et al., 2019), which could lead to the elevated concentration of CCN in the night time. Except for these two months, there are two prominent peaks in the diurnal variation of CCN, the first one in the morning (06:00–08:00 h) and the other in the evening (16:00–18:00 h). Peaks during morning hours result from anthropogenic emission and biomass burning in the nearby residential area. In contrast, the evening peaks are collectively

affected by biomass burning, vehicular emission, and air mass transport from the plains of IGP regions.

CCN diurnal variation at 0.5% SS for different seasons; M, (JAS; Aug–Sep 2018, Jun 2019), PoM (ON; Oct–Nov 2018), W (DJF; Dec 2018, Jan–Feb 2019), PrM (MAM; Mar–May 2019) is shown in Fig. 7. The average diurnal CCN concentration is recorded in PrM ($2514.7 \pm 2166.4 \text{ cm}^{-3}$) followed by W ($1712.3 \pm 862.8 \text{ cm}^{-3}$), PoM ($1645.7 \pm 690.62 \text{ cm}^{-3}$), and M ($1411.3 \pm 1110.1 \text{ cm}^{-3}$). All seasons showed two peaks, one in the morning ($\sim 06:00\text{--}08:00 \text{ h}$) and other in the evening ($18:00\text{--}20:00 \text{ h}$) for the diurnal variation, except for the PrM. M appeared relatively with a flatter diurnal pattern, although it showed a

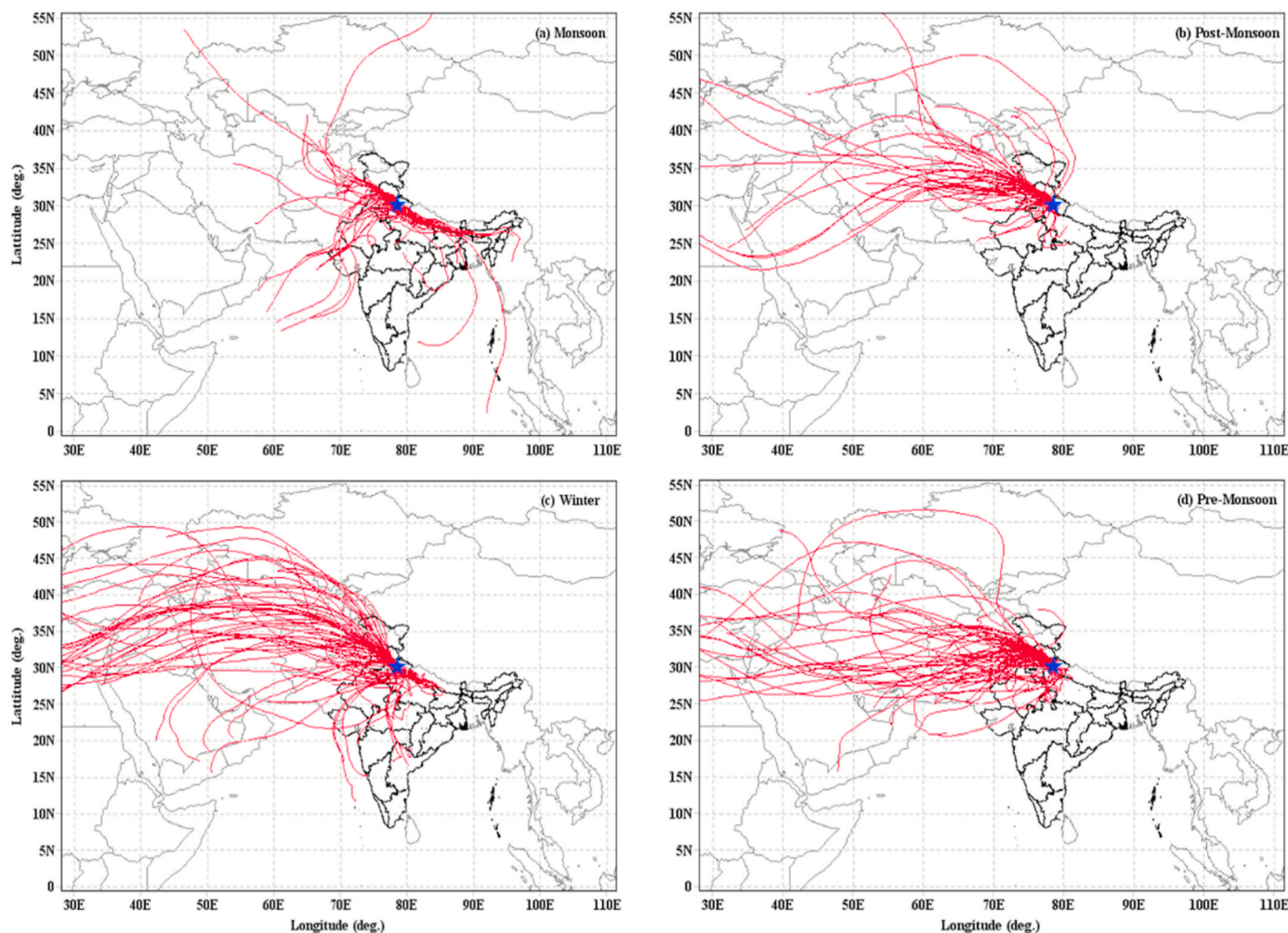


Fig. 10. Five days air mass back trajectory arriving from different regions at an altitude of 500 mAGL for (a) M(Aug – Sep 2018, Jun 2019); (b) PoM(Oct – Nov 2018); (c) W(Dec 2018, Jan – Feb 2019) and (d) PrM(Mar – May 2019) season.

slight peak in the morning (07:00–09:00 h) and the evening (18:00–20:00 h). Morning CCN peaks in PoM and W are possible due to the excessive local biomass burning emissions like wood burning in the household for cooking and heating purposes nearby the observation site. Higher RH and lower temperature profile during winter act as a driving force to condense the water-soluble VOC and organic aerosol (OA) on the surface of the particles, and additional higher aerosol, liquid water content provides a medium of aging through photo-aqueous oxidation during morning hours (Aljawhary et al., 2016; Mandariya et al., 2019). Eventually, it contributes to enhancing the hygroscopicity of the aerosol particles (Mandariya et al., 2020; Martin et al., 2013). As it was explained in section 3, that the wind activities were relatively low during the morning hours for different seasons; thus, local vehicular emission and wood-burning activities in nearby residential areas could be the major source of high concentration of aerosol loading. Furthermore, the evening CCN peak could be the result of transported air mass from the IGP regions in addition to local biomass burning emissions. The total number of fire spots for different seasons of the study period are shown in Fig. 8. Fire counts are considerably high for almost all seasons over the IGP region of the Indian subcontinent. During W and PoM season, there are higher fire activities over IGP regions, including lower Himalaya foothill regions, Pakistan, and Nepal, due to the crop residue burning and forest fire activities. For PrM season, fire activities are significantly high over the Indian subcontinent, including IGP, Nepal, North-eastern, as well as the central part of India. Carbonaceous aerosols emitted from biomass burning could act as CCN (Corrigan and Novakov,

1999; Hori et al., 2003; Pradeep Kumar et al., 2003; Roy et al., 2017), and emission from crop residue burning produces the trace gases and particulate matter (Sahai et al., 2011). It supports the increase in the CCN concentration through the nucleation and new particle formation events (Lee et al., 2019; Moorthy et al., 2011; Siingh et al., 2011). It is observed that during the PrM season, numerous biomass burning activities occurred over the IGP and Nepal regions. Also, during PoM and W season, fire count obtained high over IGP regions as a result of open field crop residue burnings and biomass burning activities over the lower Himalayan regions (Dumka et al., 2015). reported the similar pattern of diurnal variation for CCN concentration over the high altitude location of central Himalaya. However, morning peaks are prominent relative to the evening peak over the eastern Himalayan region (Roy et al., 2017) and Kanpur (Patidar et al., 2012) due to the activities of local emission of aerosol and burning of fossil fuel during the hours of heavy rush and traffic; also boundary layer dynamics play a significant role in the variation of CCN concentration (Dumka et al., 2013; Tripathi et al., 2005). Contribution of transported airmass to the observed peaks in diurnal variation of CCN concentration is explained in details using the cluster analysis of all BTs for different seasons (section 4.4).

4.3. Impact of wind pattern on CCN

Wind speed and direction play a significant role in the transportation and diffusion of atmospheric aerosols (Fast et al., 2007). The relationship of CCN loading with wind speed and direction is examined using a

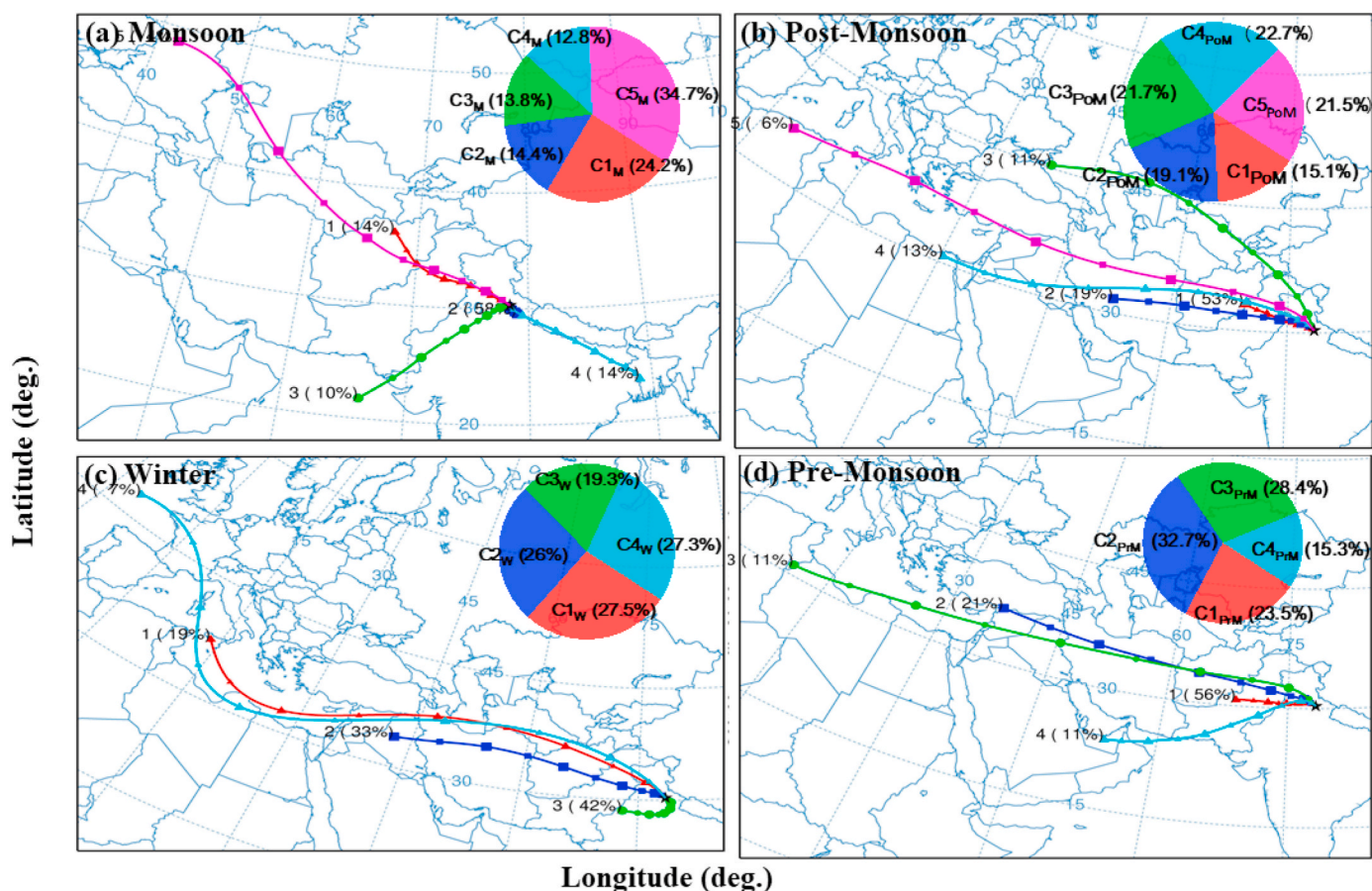


Fig. 11. Seasonal distribution of clusters of air mass trajectories arriving over the observation site (HCO) at 500 m AGL. The pie charts are showing the fractional contribution (in %) of CCN corresponding to each cluster for the averaged value of CCN concentration.

seasonally bivariate polar plot (Carslaw et al., 2006), as shown in Fig. 9. The topographic overview of the observation site shows the location of valley regions in the southeast direction to the HCO, Badshahitaul. Southwesterly winds are prevailing for almost the entire observation period. Higher concentration CCN was observed to be affected by southwesterly air mass for the M season. The highest concentrations of CCN observed for PrM season from the southeast direction, which is highly influenced by the forest fire events in the surroundings of the observation site and dust transported from the desert area of India and Arabian countries. Studies show the transport of dust particles along with other anthropogenic aerosols from southern parts of Asia, including highly polluted IGP regions, to high altitude regions of the Himalaya and Tibetan plateau (Cong et al., 2015; Gautam et al., 2009). Dust and aerosol particles may act as CCN after the mixing and coating of water-soluble sulfates and nitrates generated by the anthropogenic, industrial, and biomass burning activities in the IGP regions, as mentioned in the previous section (Li et al., 2011). Temperature gradient and strong thermal convection support the transport of aerosol and pollutants through the mountain or valley wind patterns. Several previous studies investigated the role of the valley wind pattern in the long-range transport of air mass at high altitude sites (Dumka et al., 2010, 2015; Kleissl et al., 2007; Moorthy et al., 2011; Nishita et al., 2008; Raatikainen et al., 2014; Sarangi et al., 2014; Shrestha et al., 2010). The higher value of concentration during W season could be the result of the substantial biomass burning in the surrounding residential area and vegetation and/or crop residue burning in the Garhwal Himalayan region. A shallow value of concentration is observed for the M season due to wet deposition of CCN particle by monsoonal precipitation, which also reduces the effect of long-range transported dust and aerosol (Dipu et al., 2013; Rodhe and Grandell, 1972; Singh et al., 2004).

4.4. Impact of long-range transported air mass on CCN concentration

Long-range transport of air masses and its impact on CCN concentration over the Badshahithaul region is investigated using five days air mass back trajectory arriving from different regions, ending at the altitude of 500 m AGL, which has been calculated using the HYSPLIT model for all seasons (Fig. 10).

Westerly winds mostly dominate wind patterns throughout the year from western and central Asia. Southwesterly and southeasterly winds arrive from the Arabian Sea and Bay of Bengal regions, respectively, during the monsoon season. Trajectories also contain a fraction of air mass from IGP and Nepal. Cluster analysis of BTs (Fig. 11) suggests that a large part (~60–70%) of air mass is transported from the arid and semi-arid regions of western and central Asia, including Iraq, Iran, Afghanistan, and Pakistan for W, PoM, and PrM season. While other significant fraction of the air mass from the IGP regions of the north-western part of India. During M season, less than 20% air mass is transported from central Asia, approx. 10% from the Arabian Sea region and the rest 60–70% from the east and central parts of IGP, Nepal, Bangladesh, and Bay of Bengal regions.

Cluster analysis for each hour BT of all observation days corresponding to each season of the study period is performed (Fig. 11). It suggests the potential sources of the pollutants reaching the observation site from different regions. The percentage value with each cluster shows the air mass fraction corresponding to each trajectory. The pie chart in each cluster plot shows the fraction of average CCN concentration out of the total value of CCN concentration for the individual season. Hourly averaged data corresponding to each cluster is separately plotted to explore the impact of each individual cluster on the diurnal variation of CCN concentration (Fig. 12). The highest CCN concentration

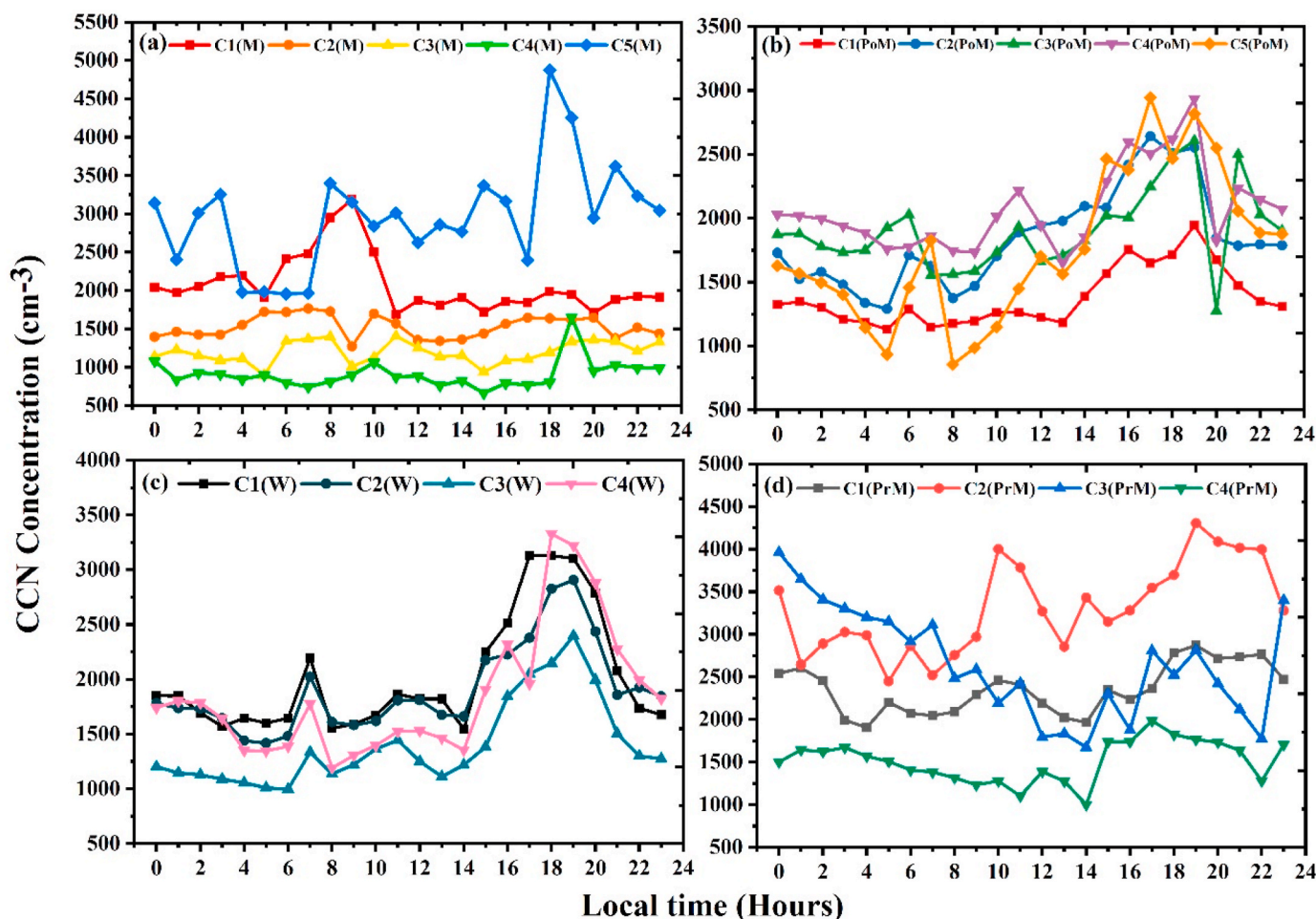


Fig. 12. Diurnal variation of CCN concentration at 0.5% SS corresponding to respective clusters for (a) M(Aug – Sep 2018, Jun 2019); (b) PoM(Oct – Nov 2018); (c) W(Dec 2018, Jan – Feb 2019) and (d) PrM(Mar – May 2019) season of the study period.

is associated with the air mass clusters (the subscript represents the corresponding season of cluster number) originating from the central and western part of Asia, containing the desert dust and continental anthropogenic pollutants for different season of the study period (Cluster ID – average CCN concentration: $C1_M - 2089.8 \text{ cm}^{-3}$, $C5_M - 2989.7 \text{ cm}^{-3}$, $C3_{PoM} - 1997 \text{ cm}^{-3}$, $C4_{PoM} - 2088.7 \text{ cm}^{-3}$, $C1_W - 1998 \text{ cm}^{-3}$, $C2_W - 1893.3 \text{ cm}^{-3}$, $C4_W - 1984.5 \text{ cm}^{-3}$, $C2_{PrM} - 3275.5 \text{ cm}^{-3}$, and $C3_{PrM} - 2840.9 \text{ cm}^{-3}$). The highest fraction of air mass was originated from the western to the central part of IGP regions and neighbouring western countries of India, i.e., Pakistan and Afghanistan ($C2_M - 1294 \text{ cm}^{-3}$; $C1_{PoM} - 1390.7 \text{ cm}^{-3}$; $C3_W - 1401 \text{ cm}^{-3}$; $C1_{PrM} - 3257.9 \text{ cm}^{-3}$). Marine influence on the air mass is noticeable ($C3_M - 1187 \text{ cm}^{-3}$; $C4_M - 1106.8 \text{ cm}^{-3}$) during the M season with the lowest CCN concentration, also for PrM ($C4_{PrM} - 1535.4 \text{ cm}^{-3}$) season from the Arabian Sea and Bay of Bengal. The diurnal pattern of PoM (Fig. 12b) shows two peaks ($\sim 06:00$ and $\sim 19:00$ h) for different clusters with the highest concentration corresponding to $C3_{PoM}$ and $C4_{PoM}$ and lowest corresponding to the $C1_{PoM}$ cluster. W season shows almost the same pattern for each cluster (Fig. 12c) with higher concentrations in the evening hours, which is also in agreement with higher wind activities in the evening hours. Diurnal variation of PrM season (Fig. 12d) show unconventional patterns with several peaks at different hours. $C2_{PrM}$ and $C3_{PrM}$ cluster contribute to the observed higher value of CCN at night hours. Previous studies (Datta et al., 2010; Xue et al., 2013) suggested that the transported polluted air mass from urban and industrial areas of Eurasia and the Gulf countries contains Asian dust, VOCs, and anthropogenic pollutants. Chemical characterization of pollutants over IGP

regions also suggest that during biomass (agricultural waste, biofuel, and crop residue) burning emission enhance the concentration of fine mode aerosols (Rajput et al., 2014a, 2014b, 2016; Rastogi et al., 2014; Singh et al., 2014) which eventually got transported to the higher Himalayan regions through the trans-Himalayan valleys by up-valley flow (Dhungel et al., 2018). During the monsoon, the significant impact of marine air mass leads to the decreased concentration of pollutants (Datta et al., 2010), reaching the central Himalaya through the wet scavenging process due to heavy moisture content.

CWTs were calculated to identify regional source areas affecting the CCN concentration over the Badshahithaul region (Fig. 13). CWTs are color-coded, plotted over the Southern part of Asia (Indian continent region) to highlight the major potential sources of air mass transport and corresponding CCN concentration. It is observed that higher concentrations of CCN are being transported at the observation site with the air masses arriving from the central and western parts of Asia. It consists of dust particles from the west Asian countries. Previous studies (Adak et al., 2014; Gautam et al., 2009) reported the long-range transport of desert dust over the high altitude regions of the Himalaya. A large fraction of air mass with CCN concentration $\sim 2000 \text{ cm}^{-3}$ arrives from the northern and central parts of IGP for different seasons of the study period. It is also reaching the observation site from the Nepal region during the M and W season. Although a large fraction of the air mass is coming from the Arabian Sea, Bangladesh, and Bay of Bengal is corresponding to the very low ($<1000 \text{ cm}^{-3}$) concentration of CCN for M season.

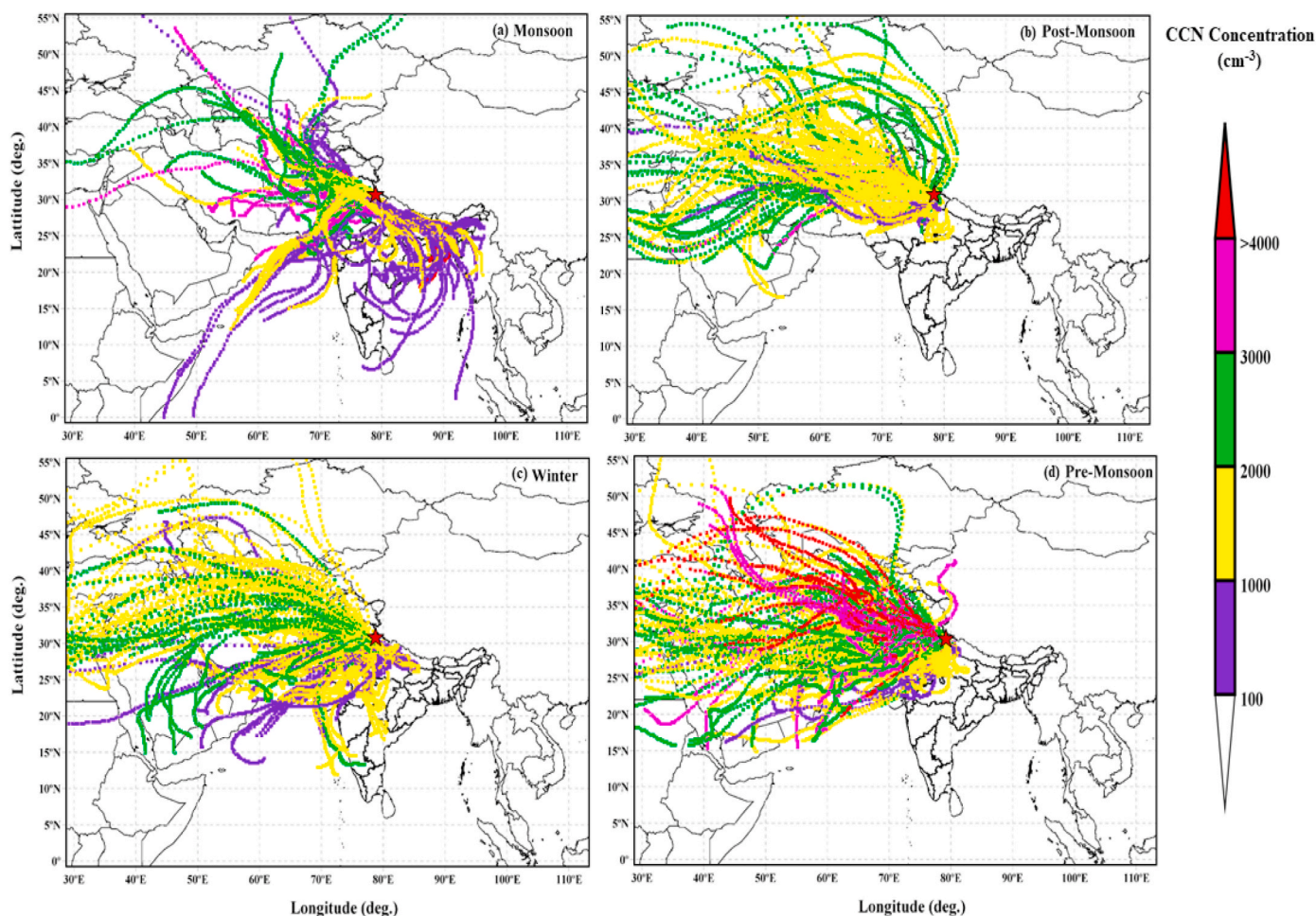


Fig. 13. Concentrated Weighted Trajectories for CCN concentration of (a) M(Aug – Sep 2018, Jun 2019); (b) PoM(Oct – Nov 2018); (c) W(Dec 2018, Jan – Feb 2019) and (d) PrM(Mar – May 2019) season.

4.5. Comparisons with other Indian subcontinent sites

Our present study is compared with the other similar studies carried out in the different regions of India, under a variety of climatic conditions along with the various geographical conditions. The comparative concentration values for CCN for different sites of India are listed in Table 1.

Nainital (1958 m AMSL) is the nearest observation site, and it has somewhat similar geography and climatic condition as that of HCO. Both observation sites are situated at high altitude hill stations of the Western Himalayan region of Uttarakhand. A higher value of concentration is obtained for M season at our site than that for Nainital (Dumka et al., 2015; Gogoi et al., 2015). One of the possible reasons for the higher concentration at our site could be the high loading of aerosols in the first weeks of Jun 2019 due to intensive biomass burning activities and forest fire events over the Garhwal Himalayan region, as mentioned in section 4.1 while it is almost the same for the W season at both observation sites. Darjeeling is also a high-altitude station of the eastern Himalayan region showing a similar seasonal variation of CCN. But the values for this station are comparatively low to our location (Roy et al., 2017). A long-range transport study of aerosol transfer suggested that HCO location is in the close vicinity to the highly polluted regions of IGP and influenced by the dust and aerosol transferred from and western Asian countries.

Kanpur shows a very high concentration (almost double) compared to the values observed at HCO. As being a representative urban site of IGP, it is highly influenced by anthropogenic, vehicular, and industrial

emission (Bhattu and Tripathi, 2014). On the other hand, the relatively high value of CCN concentration is reported for Thumba (3 m AMSL) on the coastal region of the Western Ghats in peninsular India during the summer monsoon season (Jayachandran et al., 2017). The air mass over this site is supplied from the Indian Ocean region containing moisture and natural sea salt particles. The carbonaceous sources from the nearby urban sources contribute to the high concentration of CCN. Another study by (Jayachandran et al., 2018) compares the concentration of CCN at the coastal region of western ghat and a hill station site Ponmudi (960 m AMSL) where carbonaceous combustion sources highly influence the CCN concentration. Higher concentration at day time and low at night opposite in contrast to the coastal site (Thumba). Mahabaleshwar (1348 m AMSL) is a high-altitude site in the western ghats of India. The CCN concentration for this site was observed higher during monsoon due to local emission and biogenic VOC emission despite the dominant sink process due to the monsoon washout mechanism. The Winter season is highly influenced by the anthropogenic aerosol and calm winds (Leena et al., 2015). These comparative analyses suggest that IGP is abundantly polluted and source of aerosols generated in the locality or accumulated from other regions through different means of transport. These pollutants get transported to high altitude areas through up slope valley or mountain breeze. The effect of this transported aerosol containing air mass decreases on moving from western to eastern Himalayan regions.

5. Conclusion

The present study of CCN concentration over the Garhwal Himalayan

Table 1

Comparison of the present study with other similar studies over different regions of India.

Sampling location (Coordinates; elevation a.m.s.l.)	Condition	Sampling Period	N_{CCN} (cm^{-3})	Reference
Swami Ram Tirth (SRT) Campus Badshahithaul H. N. B. Garhwal University (30.34 N, 78.41 E; 1706 m)	Monsoon	Aug–Sept 2018, June 2019	1411.3 ± 1110.1 at 0.5% SS	Present Study
	Post-Monsoon	Oct–Nov 2018	1645.7 ± 690.62 at 0.5% SS	
	Winter	Dec 2018, Jan–Feb 2019	1712.3 ± 862.8 at 0.5% SS	
	Pre-Monsoon	Mar–May 2019	2514.7 ± 2166.4 at 0.5% SS	
Nanital (29.2 N, 79.3 E; 1960 m)	Monsoon	June–Aug 2011	1063.59 ± 10.39 at 0.46% SS	Gogoi et al. (2015)
	Autumn	Sept–Oct 2011	1935.44 ± 14.46 at 0.46% SS	
	Winter	Dec 2011, Jan–Feb 2012	2180.14 ± 16.05 at 0.46% SS	
Nanital (29.4 N, 79.5 E; 1958 m)	Monsoon	Jun–Aug 2011	836 ± 618 at 0.3% SS	Dumka et al. (2015)
	Post-Monsoon	Sept–Nov 2011	1630 ± 560 0.3% SS	
	Winter	Dec 2011, Jan–Feb 2012	1590 ± 892 at 0.3% SS	
	Pre-Monsoon	Mar 2012	2065 ± 476 at 0.3%	
Darjeeling (27.01 N, 88.15 E; 2200 m)	Post-Monsoon	Oct–Nov 2015	887 ± 295 at 0.5% SS	Roy et al. (2017)
	Winter	Dec 2015, Jan–Feb 2016	1652 ± 694 at 0.5% SS	
	Pre-Monsoon	Mar–May 2016	1998 ± 862 at 0.5% SS	
	Western Ghats Monsoon	Jul–Sep 2016	474 ± 318 at 0.4% SS	
Ponmudi (8.8 N, 77.1 E; 960 m) Kanpur (26.5 N, 80.3 E; 142 m)	Spring	Mar 2012	3899 at 0.5% SS	Jayachandran et al. (2018) Bhattu and Tripathi (2014)
	Summer	May–June 2012	5074 at 0.5% SS	
	Monsoon	Aug 2012	3014 at 0.5% SS	
	Monsoon	June–Aug 2012	~ 1800 at 0.6% SS	
Mahabaleshwar (17.56 N, 73.4 E; 1348 m)	Winter	Dec 2012, Jan–Feb 2013	~ 1600 at 0.6% SS	Leena et al. (2015)
	Pre-Monsoon	Mar–May 2013	~ 1700 at 0.6% SS	
	Monsoon	Jun–Sept 2013	2096 ± 834 at 0.4% SS	
Thumba (8.54 N, 76.88 E; 3 m)	Monsoon	Jun–Sept 2014	1529 ± 411 at 0.4% SS	Jayachandran et al. (2017)

region investigates the variation of CCN, possible emission sources, transport, and the removal of aerosol particles from the atmosphere and its dependency on meteorological parameters and local geography. Outcomes of this study are listed as follow:

- Simultaneous measurement of CCN concentration (Aug 01, 2018–Jun 30, 2019) and meteorological parameters (Sep 01, 2018–Jun 30, 2018) carried out at HCO. An increase in the concentration was observed from M to PrM season with a vast range of variation in the concentration values.
- Two peaks pattern observed in the diurnal variation of CCN concentration is supposed to be caused by local sources (such as vehicular emission, biomass burning) and long-range transport of aerosol and precursor gases, which could lead to gas to particle conversion, nucleation, and new particle formation in the influence of high temperature and solar radiation.
- Exceedingly high values of CCN concentration (with an average of 3842.9 cm^{-3}) in the month of May 2019 was a result of elevated fire activities in northern India. It was comparatively double to the average concentration of CCN for the rest of the months (1637.7 cm^{-3}). Higher values of fire counts (~ 150 counts/day) support the enormous increase of CCN concentration during the HFAD up to the highest value of the whole observation period (10649.99 cm^{-3} on May 30, 2019) over the Uttarakhand region.
- Cluster analysis suggests that the higher concentration (more than 50% of the fraction) of CCN corresponds to the air mass arriving from the western and central regions of Asia. Although, the fraction of air mass corresponding to the above-mentioned clusters was significantly low. Clusters arriving from the marine or subcontinent regions contain the lowest fraction ($\sim 25\%$ in monsoon and $\sim 15\%$ in pre-monsoon season) of CCN concentration.
- Events such as rainfall, snowfall, biomass burning, and fire forest significantly influence the concentration of CCN particles and can change its value drastically higher or lower than the average concentration of CCN.
- Air mass back trajectories and CWTs suggest the contribution of possible sources of air mass containing various pollutant transported over the observation site (HCO). Along with the dust particles from desert areas of western India and western Asian countries (with concentration more than 2000 cm^{-3} of N_{CCN}), crop residue burning in

the west and central parts of IGP and vegetation/forest fire contributes to the loading of aerosol responsible for the formation and activation of CCN over high altitude hilltops of Western Himalayan region.

- IGP is the reservoir of a large amount of aerosol generated due to industrialization, anthropogenic, and natural activities. Upslope valley wind patterns sweep up the aerosol to the high altitude and act as CCN after aging and mixing with the water-soluble nitrates and sulfates.

CRedit authorship contribution statement

Alok Sagar Gautam: Conceptualization, Data analysis and Formulation. **S.N. Tripathi:** Conceptualization, Data interpretation. **Abhishek Joshi:** Data collection and analysis. **Anil Kumar Mandariya:** Instrumentation and quality control. **Karan Singh:** Review and editing. **Gaurav Mishra:** Instrumentation, editing. **Sanjeev Kumar:** Data interpretation. **R.C. Ramola:** Visualization of the figures and tables.

Declaration of competing interest

The authors declare that they have no known competing financial interests or personal relationships that could have appeared to influence the work reported in this paper.

Acknowledgment

Dr. A. S. Gautam and other Authors would like to thank the Department of Science and Technology, Government of India for funding support under, Climate Change Programme (CCP), SPLICE Division, Department of Science & Technology, Technology Bhavan, New Mehrauli Road, New Delhi-110 016 (DST/CCP/Aerosol/83/2017(G)). ASG would like to thank Vice – Chancellor, HNBGU Srinagar, Director-SRT Campus, HNBGU Srinagar, and Head, Department of Physics, HNBGU Srinagar for providing the necessary infrastructure facility and guidance for this study. Authors would like to thank Dr. Deepika Bhattu, Assistant Professor in Civil and Infrastructure Engineering, IIT Jodhpur, India, to provide a MATLAB code for DMA transfer function and multi-charge correction, and cumulative Gaussian distribution function fitting (CDF) of CCN efficiency spectra. ASG would like to thank Dr. Vijay P.

Kanawade, University Centre for Earth and Space Sciences (UCESS), University of Hyderabad and Akash Kumar for providing help in laboratory establishment and data analysis.

Appendix A. Supplementary data

Supplementary data related to this article can be found at <https://doi.org/10.1016/j.atmosenv.2020.118123>.

References

- Adak, A., Chatterjee, A., Singh, A.K., Sarkar, C., Ghosh, S., Raha, S., 2014. Atmospheric fine mode particulates at eastern Himalaya, India: role of meteorology, long-range transport and local anthropogenic sources. *Aerosol Air Qual. Res.* 14, 440–450. <https://doi.org/10.4209/aaqr.2013.03.0090>.
- Aljawhary, D., Zhao, R., Lee, A.K.Y., Wang, C., Abbott, J.P.D., 2016. Kinetics, mechanism, and secondary organic aerosol yield of aqueous phase photo-oxidation of α -pinene oxidation products. *J. Phys. Chem. A* 120, 1395–1407. <https://doi.org/10.1021/acs.jpca.5b06237>.
- Almeida, G.P., Brito, J., Morales, C.A., Andrade, M.F., Artaxo, P., 2014. Measured and modelled cloud condensation nuclei (CCN) concentration in São Paulo, Brazil: the importance of aerosol size-resolved chemical composition on CCN concentration prediction. *Atmos. Chem. Phys.* 14, 7559–7572. <https://doi.org/10.5194/acp-14-7559-2014>.
- Bhardwaj, P., Naja, M., Rupakheti, M., Lupascu, A., Mues, A., Kumar Panday, A., Kumar, R., Singh Mahata, K., Lal, S., Chandola, H.C., Lawrence, M.G., 2018. Variations in surface ozone and carbon monoxide in the Kathmandu Valley and surrounding broader regions during SusKat-ABC field campaign: role of local and regional sources. *Atmos. Chem. Phys.* 18, 11949–11971. <https://doi.org/10.5194/acp-18-11949-2018>.
- Bhattu, D., Tripathi, S.N., 2015. CCN closure study: Effects of aerosol chemical composition and mixing state. *120(2)*. *Journal of Geophysical Research*, pp. 766–783. <https://doi.org/10.1002/2014JD021978>.
- Bhattu, D., Tripathi, S.N., 2014. Inter-seasonal variability in size-resolved CCN properties at Kanpur, India. *Atmos. Environ.* 85, 161–168. <https://doi.org/10.1016/j.atmosenv.2013.12.016>.
- Bonasoni, P., Laj, P., Marinoni, A., Sprenger, M., Angelini, F., Arduini, J., Bonafè, U., Calzolari, F., Colombo, T., Decesari, S., Di Biagio, C., di Sarra, A.G., Evangelisti, F., Duchi, R., Facchini, M., Fuzzi, S., Gobbi, G.P., Maione, M., Panday, A., Roccatto, F., Sellegri, K., Venzac, H., Verza, G., Villani, P., Vuillermoz, E., Cristofanelli, P., 2010. Atmospheric Brown Clouds in the Himalayas: first two years of continuous observations at the Nepal Climate Observatory-Pyramid (5079 m). *Atmos. Chem. Phys.* 10, 7515–7531. <https://doi.org/10.5194/acp-10-7515-2010>.
- Borys, R.D., Lowenthal, D., Mitchell, D.L., 1996. CCN Regulation of snowfall rates. *Nucleation and Atmospheric Aerosols 1996*. Elsevier, pp. 808–811. <https://doi.org/10.1016/B978-008042030-1/50195-5>.
- Bougiatioti, A., Argyrouli, A., Solomos, S., Vratolis, S., Eleftheriadis, K., Papayannis, A., Nenes, A., 2017. CCN activity, variability and influence on droplet formation during the HygrA-Cd campaign in Athens. *Atmosphere* 8, 108. <https://doi.org/10.3390/atmos8060108>.
- Carslaw, D., Beevers, S., Ropkins, K., Bell, M., 2006. Detecting and quantifying aircraft and other on-airport contributions to ambient nitrogen oxides in the vicinity of a large international airport. *Atmos. Environ.* 40, 5424–5434. <https://doi.org/10.1016/j.atmosenv.2006.04.062>.
- CENSUS, 2011. *Census of India Website. Office of the Registrar General & Census Commissioner, India*.
- Che, H.C., Zhang, X.Y., Wang, Y.Q., Zhang, L., Shen, X.J., Zhang, Y.M., Ma, Q.L., Sun, J.Y., Zhang, Y.W., Wang, T.T., 2016. Characterization and parameterization of aerosol cloud condensation nuclei activation under different pollution conditions. *Sci. Rep.* 6, 1–14. <https://doi.org/10.1038/srep24497>.
- Cong, Z., Kawamura, K., Kang, S., Fu, P., 2015. Penetration of biomass-burning emissions from South Asia through the Himalayas: new insights from atmospheric organic acids. *Sci. Rep.* 5, 9580. <https://doi.org/10.1038/srep09580>.
- Corrigan, C.E., Novakov, T., 1999. Cloud condensation nucleus activity of organic compounds: a laboratory study. *Atmos. Environ.* 33, 2661–2668. [https://doi.org/10.1016/S1352-2310\(98\)00310-0](https://doi.org/10.1016/S1352-2310(98)00310-0).
- Crosbie, E., Youn, J.-S., Balch, B., Wonauschütz, A., Shingler, T., Wang, Z., Conant, W.C., Betterton, E.A., Sorooshian, A., 2015. On the competition among aerosol number, size and composition in predicting CCN variability: a multi-annual field study in an urbanized desert. *Atmos. Chem. Phys.* 15, 6943–6958. <https://doi.org/10.5194/acp-15-6943-2015>.
- Datta, A., Saud, T., Goel, A., Tiwari, S., Sharma, S.K., Saxena, M., Mandal, T.K., 2010. Variation of ambient SO₂ over Delhi. *J. Atmos. Chem.* 65, 127–143. <https://doi.org/10.1007/s10874-011-9185-2>.
- DCMSME, 2016. *Development Commissioner Ministry of Micro, Small & Medium Enterprises [WWW Document]*. <http://www.dcmsme.gov.in/AnnualReport-Tcs.html>. http://dcmsme.gov.in/dips/U.K_dipr.html.
- Devi, J.J., Tripathi, S.N., Gupta, T., Singh, B.N., Gopalakrishnan, V., Dey, S., 2011. Observation-based 3-D view of aerosol radiative properties over Indian Continental Tropical Convergence Zone: implications to regional climate. *Tellus B* 63, 971–989. <https://doi.org/10.1111/j.1600-0889.2011.00580.x>.
- Dey, S., Di Girolamo, L., 2010. A climatology of aerosol optical and microphysical properties over the Indian subcontinent from 9 years (2000–2008) of Multiangle Imaging Spectroradiometer (MISR) data. *J. Geophys. Res.* 115, D15204. <https://doi.org/10.1029/2009JD013395>.
- Dhungel, S., Kathayat, B., Mahata, K., Panday, A., 2018. Transport of regional pollutants through a remote trans-Himalayan valley in Nepal. *Atmos. Chem. Phys.* 18, 1203–1216. <https://doi.org/10.5194/acp-18-1203-2018>.
- Dipu, S., Prabha, T.V., Pandithurai, G., Dudhia, J., Pfister, G., Rajesh, K., Goswami, B.N., 2013. Impact of elevated aerosol layer on the cloud macrophysical properties prior to monsoon onset. *Atmos. Environ.* 70, 454–467. <https://doi.org/10.1016/j.atmosenv.2012.12.036>.
- Draxler, R., Stunder, B., Rolph, G., Stein, A., Taylor, A., 2014. *HYSPLIT4 User's Guide Version 4 - Last Revision: September 2014*.
- Dumka, U.C., Bhattu, D., Tripathi, S.N., Kaskaoutis, D.G., Madhavan, B.L., 2015. Seasonal inhomogeneity in cloud precursors over Gangetic Himalayan region during GVAX campaign. *Atmos. Res.* 155, 158–175. <https://doi.org/10.1016/j.atmosres.2014.11.022>.
- Dumka, U.C., Manchanda, R.K., Sinha, P.R., Sreenivasan, S., Moorthy, K.K., Suresh Babu, S., 2013. Temporal variability and radiative impact of black carbon aerosol over tropical urban station Hyderabad. *J. Atmos. Solar-Terrestrial Phys.* 105–106, 81–90. <https://doi.org/10.1016/j.jastp.2013.08.003>.
- Dumka, U.C., Moorthy, K.K., Kumar, R., Hegde, P., Sagar, R., Pant, P., Singh, N., Babu, S., 2010. Characteristics of aerosol black carbon mass concentration over a high altitude location in the Central Himalayas from multi-year measurements. *Atmos. Res.* 96, 510–521. <https://doi.org/10.1016/j.atmosres.2009.12.010>.
- Dusek, U., Frank, G.P., Hildebrandt, L., Curtius, J., Schneider, J., Walter, S., Chand, D., Drewnick, F., Hings, S., Jung, D., Borrmann, S., Andreae, M.O., 2006. Size matters more than chemistry for cloud-nucleating ability of aerosol particles. *Science (80-)* 312, 1375–1378. <https://doi.org/10.1126/science.1125261>.
- Ervens, B., Cubison, M., Andrews, E., Feingold, G., Ogren, J.A., Jimenez, J.L., DeCarlo, P., Nenes, A., 2007. Prediction of cloud condensation nucleus number concentration using measurements of aerosol size distributions and composition and light scattering enhancement due to humidity. *J. Geophys. Res. Atmos.* 112, 1–15. <https://doi.org/10.1029/2006JD007426>.
- Fast, J.D., de Foy, B., Acevedo Rosas, F., Caetano, E., Carmichael, G., Emmons, L., McKenna, D., Mena, M., Skamarock, W., Tie, X., Coulter, R.L., Barnard, J.C., Wiedinmyer, C., Madronich, S., 2007. A meteorological overview of the MILAGRO field campaigns. *Atmos. Chem. Phys. Discuss.* 7, 2037–2089. <https://doi.org/10.5194/acpd-7-2037-2007>.
- Finlayson-Pitts, B.J., 1997. Tropospheric air pollution: ozone, airborne toxics, polycyclic aromatic hydrocarbons, and particles. *Science* 276, 1045–1051. <https://doi.org/10.1126/science.276.5315.1045>.
- Garrett, T.J., Avey, L., Palmer, P.I., Stohl, A., Neuman, J.A., Brock, C.A., Ryerson, T.B., Holloway, J.S., 2006. Quantifying wet scavenging processes in aircraft observations of nitric acid and cloud condensation nuclei. *J. Geophys. Res. Atmos.* 111, 1–12. <https://doi.org/10.1029/2006JD007416>.
- Gautam, A.S., Singh, D., Kamra, A.K., 2017. Statistical analysis of the atmospheric ion concentrations and mobility distributions at a tropical station. *Pune. Q. J. R. Meteorol. Soc.* 143, 2116–2128. <https://doi.org/10.1002/qj.3071>.
- Gautam, R., Hsu, N.C., Tsay, S.C., Lau, K.M., Holben, B., Bell, S., Smirnov, A., Li, C., Hansell, R., Ji, Q., Payra, S., Aryal, D., Kayastha, R., Kim, K.M., 2011. Accumulation of aerosols over the Indo-Gangetic plains and southern slopes of the Himalayas: distribution, properties and radiative effects during the 2009 pre-monsoon season. *Atmos. Chem. Phys.* 11, 12841–12863. <https://doi.org/10.5194/acp-11-12841-2011>.
- Gautam, R., Liu, Z., Singh, R.P., Hsu, N.C., 2009. Two contrasting dust-dominant periods over India observed from MODIS and CALIPSO data. *Geophys. Res. Lett.* 36, L06813. <https://doi.org/10.1029/2008GL036967>.
- Gogoi, M.M., Babu, S.S., Jayachandran, V., Moorthy, K.K., Sathesh, S.K., Naja, M., Kotamarthi, V.R., 2015. Optical properties and CCN activity of aerosols in a high-altitude Himalayan environment: results from RAWEX-GVAX. *J. Geophys. Res.* Atmos. 120, 2453–2469. <https://doi.org/10.1002/2014JD022966>.
- Haywood, J., 2016. *Atmospheric aerosols and their role in climate change. Climate Change: Observed Impacts on Planet Earth*, second ed. Elsevier B.V. <https://doi.org/10.1016/B978-0-444-63524-2.00027-0>.
- Hori, M., Ohta, S., Murao, N., Yamagata, S., 2003. Activation capability of water soluble organic substances as CCN. *J. Aerosol Sci.* 34, 419–448. [https://doi.org/10.1016/S0021-8502\(02\)00190-8](https://doi.org/10.1016/S0021-8502(02)00190-8).
- Hsu, Y.-K., Holsen, T.M., Hopke, P.K., 2003. Comparison of hybrid receptor models to locate PCB sources in Chicago. *Atmos. Environ.* 37, 545–562. [https://doi.org/10.1016/S1352-2310\(02\)00886-5](https://doi.org/10.1016/S1352-2310(02)00886-5).
- Hudson, J.G., 2007. Variability of the relationship between particle size and cloud-nucleating ability. *Geophys. Res. Lett.* 34, 1–5. <https://doi.org/10.1029/2006GL028850>.
- IPCC, 2014. *Intergovernmental Panel on Climate Change*. Cambridge University Press, Cambridge. <https://doi.org/10.1017/cbo9781107415416>.
- Jayachandran, V., Nair, V.S., Babu, S.S., 2018. CCN activation properties at a tropical hill station in Western Ghats during south-west summer monsoon: vertical heterogeneity. *Atmos. Res.* 214, 36–45. <https://doi.org/10.1016/j.atmosres.2018.07.018>.
- Jayachandran, V., Nair, V.S., Babu, S.S., 2017. CCN characteristics over a tropical coastal station during south-west monsoon: observations and closure studies. *Atmos. Environ.* 164, 299–308. <https://doi.org/10.1016/j.atmosenv.2017.06.012>.
- Jefferson, A., 2010. Empirical estimates of CCN from aerosol optical properties at four remote sites. *Atmos. Chem. Phys.* 10, 6855–6861. <https://doi.org/10.5194/acp-10-6855-2010>.
- Kanawade, V.P., Tripathi, S.N., Singh, D., Gautam, A.S., Srivastava, A.K., Kamra, A.K., Soni, V.K., Sethi, V., 2014. Observations of new particle formation at two distinct

- Indian subcontinental urban locations. *Atmos. Environ.* 96, 370–379. <https://doi.org/10.1016/j.atmosenv.2014.08.001>.
- Kedia, S., Ramachandran, S., Holben, B.N., Tripathi, S.N., 2014. Quantification of aerosol type, and sources of aerosols over the Indo-Gangetic Plain. *Atmos. Environ.* 98, 607–619. <https://doi.org/10.1016/j.atmosenv.2014.09.022>.
- Khalizov, A.F., Lin, Y., Qiu, C., Guo, S., Collins, D., Zhang, R., 2013. Role of OH-initiated oxidation of isoprene in aging of combustion soot. *Environ. Sci. Technol.* 47, 2254–2263. <https://doi.org/10.1021/es3045339>.
- Kleissl, J., Honrath, R.E., Dziobak, M.P., Tanner, D., Val Martín, M., Owen, R.C., Helmig, D., 2007. Occurrence of upslope flows at the Pico mountain top observatory: a case study of orographic flows on a small, volcanic island. *J. Geophys. Res. Atmos.* 112, 1–16. <https://doi.org/10.1029/2006JD007565>.
- Kumar, R., Naja, M., Satheesh, S.K., Ojha, N., Joshi, H., Sarangi, T., Pant, P., Dumka, U. C., Hegde, P., Venkataramani, S., 2011. Influences of the springtime northern Indian biomass burning over the central Himalayas. *J. Geophys. Res. Atmos.* 116, 1–14. <https://doi.org/10.1029/2010JD015509>.
- Lance, S., Nenes, A., Medina, J., Smith, J.N., 2006. Mapping the operation of the DMT continuous flow CCN counter. *Aerosol Sci. Technol.* 40, 242–254. <https://doi.org/10.1080/02786820500543290>.
- Lee, S.-H., Gordon, H., Yu, H., Lehtipalo, K., Haley, R., Li, Y., Zhang, R., 2019. New particle formation in the atmosphere: from molecular clusters to global climate. *J. Geophys. Res. Atmos.* 124, 7098–7146. <https://doi.org/10.1029/2018JD029356>.
- Leena, P.P., Pandithurai, G., Anilkumar, V., Murugavel, P., Sonbawne, S.M., Dani, K.K., 2015. Seasonal variability in aerosol, CCN and their relationship observed at a high altitude site in Western Ghats. *Meteorol. Atmos. Phys.* 128, 143–153. <https://doi.org/10.1007/s00703-015-0406-0>.
- Li, J., Fu, Q., Huo, J., Wang, D., Yang, W., Bian, Q., Duan, Y., Zhang, Y., Pan, J., Lin, Y., Huang, K., Bai, Z., Wang, S.H., Fu, J.S., Louie, P.K.K., 2015. Tethered balloon-based black carbon profiles within the lower troposphere of Shanghai in the 2013 East China smog. *Atmos. Environ.* 123, 327–338. <https://doi.org/10.1016/j.atmosenv.2015.08.096>.
- Li, W., Li, P., Sun, G., Zhou, S., Yuan, Q., Wang, W., 2011. Cloud residues and interstitial aerosols from non-precipitating clouds over an industrial and urban area in northern China. *Atmos. Environ.* 45, 2488–2495. <https://doi.org/10.1016/j.atmosenv.2011.02.044>.
- Lüthi, Z.L., Škerlak, B., Kim, S.-W., Lauer, A., Mues, A., Rupakheti, M., Kang, S., 2014. Atmospheric brown clouds reach the Tibetan Plateau by crossing the Himalayas. *Atmos. Chem. Phys. Discuss.* 14, 28105–28146. <https://doi.org/10.5194/acpd-14-28105-2014>.
- Mandariya, A.K., Gupta, T., Tripathi, S.N., 2019. Effect of aqueous-phase processing on the formation and evolution of organic aerosol (OA) under different stages of fog life cycles. *Atmos. Environ.* 206, 60–71. <https://doi.org/10.1016/j.atmosenv.2019.02.047>.
- Mandariya, A.K., Tripathi, S.N., Gupta, T., Mishra, G., 2020. Wintertime hygroscopic growth factors (HGFs) of accumulation mode particles and their linkage to chemical composition in a heavily polluted urban atmosphere of Kanpur at the Centre of IGP, India: impact of ambient relative humidity. *Sci. Total Environ.* 704 <https://doi.org/10.1016/j.scitotenv.2019.135363>.
- Martin, M., Tritscher, T., Jurányi, Z., Heringa, M.F., Sierau, B., Weingartner, E., Chirico, R., Gysel, M., Prévôt, A.S.H., Baltensperger, U., Lohmann, U., 2013. Hygroscopic properties of fresh and aged wood burning particles. *J. Aerosol Sci.* 56, 15–29. <https://doi.org/10.1016/j.jaerosci.2012.08.006>.
- Miao, Y., Li, J., Miao, S., Che, H., Wang, Y., Zhang, X., Zhu, R., Liu, S., 2019. Interaction between planetary boundary layer and PM_{2.5} pollution in megacities in China: a review. *Curr. Pollut. Reports* 5, 261–271. <https://doi.org/10.1007/s40726-019-00124-5>.
- Moorthy, K.K., Sreekanth, V., Prakash Chaubey, J., Gogoi, M.M., Suresh Babu, S., Kumar Kompalli, S., Bagare, S.P., Bhatt, B.C., Gaur, V.K., Prabhu, T.P., Singh, N.S., 2011. Fine and ultrafine particles at a near-free tropospheric environment over the high-altitude station Hanle in the Trans-Himalaya: new particle formation and size distribution. *J. Geophys. Res.* 116, D20212. <https://doi.org/10.1029/2011JD016343>.
- Nishita, C., Osada, K., Kido, M., Matsunaga, K., Iwasaka, Y., 2008. Nucleation mode particles in upslope valley winds at Mount Norikura, Japan: implications for the vertical extent of new particle formation events in the lower troposphere. *J. Geophys. Res.* 113, D06202. <https://doi.org/10.1029/2007JD009302>.
- Panicker, A.S., Sandeep, K., Negi, R.S., Gautam, A.S., Bisht, D.S., Beig, G., Murthy, B.S., Latha, R., Singh, S., Das, S., 2019. Estimates of carbonaceous aerosol radiative forcing over a semiurban environment in Garhwal Himalayas. *Pure Appl. Geophys.* 176, 5069–5078. <https://doi.org/10.1007/s00024-019-02248-7>.
- Patidar, V., Tripathi, S.N., Bharti, P.K., Gupta, T., 2012. First surface measurement of cloud condensation nuclei over Kanpur, IGP: role of long range transport. *Aerosol Sci. Technol.* 46, 973–982. <https://doi.org/10.1080/02786826.2012.685113>.
- Pradeep Kumar, P., Broekhuizen, K., Abbatt, J.P.D., 2003. Organic acids as cloud condensation nuclei: laboratory studies of highly soluble and insoluble species. *Atmos. Chem. Phys.* 3, 509–520. <https://doi.org/10.5194/acp-3-509-2003>.
- Pruppacher, H.R., Klett, J.D., 1997. *Microphysics of Clouds and Precipitation*, 2nd ed., 18. *Atmospheric and Oceanographic Sciences Library*, Springer, New York, p. 954.
- Raatikainen, T., Hyvärinen, A.-P., Hatakka, J., Panwar, T.S., Hooda, R.K., Sharma, V.P., Lihavainen, H., 2014. The effect of boundary layer dynamics on aerosol properties at the Indo-Gangetic plains and at the foothills of the Himalayas. *Atmos. Environ.* 89, 548–555. <https://doi.org/10.1016/j.atmosenv.2014.02.058>.
- Rajput, P., Mandariya, A., Kachawa, L., Singh, D.K., Singh, A.K., Gupta, T., 2016. Chemical characterisation and source apportionment of PM₁ during massive loading at an urban location in Indo-Gangetic Plain: impact of local sources and long-range transport. *Tellus Ser. B Chem. Phys. Meteorol.* 68 <https://doi.org/10.3402/tellusb.v68.30659>.
- Rajput, P., Sarin, M., Sharma, D., Singh, D., 2014a. Characteristics and emission budget of carbonaceous species from post-harvest agricultural-waste burning in source region of the Indo-Gangetic plain. *Tellus Ser. B Chem. Phys. Meteorol.* 66 <https://doi.org/10.3402/tellusb.v66.21026>.
- Rajput, P., Sarin, M.M., Sharma, D., Singh, D., 2014b. Atmospheric polycyclic aromatic hydrocarbons and isomer ratios as tracers of biomass burning emissions in Northern India. *Environ. Sci. Pollut. Res.* 21, 5724–5729. <https://doi.org/10.1007/s11356-014-2496-5>.
- Ram, K., Tripathi, S.N., Sarin, M.M., Bhattu, D., 2014. Primary and secondary aerosols from an urban site (Kanpur) in the Indo-Gangetic Plain: impact on CCN, CN concentrations and optical properties. *Atmos. Environ.* 89, 655–663. <https://doi.org/10.1016/j.atmosenv.2014.02.009>.
- Ramanathan, V., Chung, C., Kim, D., Bettge, T., Buja, L., Kiehl, J.T., Washington, W.M., Fu, Q., Sikka, D.R., Wild, M., 2005. Atmospheric brown clouds: impacts on South Asian climate and hydrological cycle. *Proc. Natl. Acad. Sci. Unit. States Am.* 102, 5326–5333. <https://doi.org/10.1073/pnas.0500656102>.
- Ramanathan, V., Crutzen, P.J., Lelieveld, J., Mitra, A.P., Althausen, D., Anderson, J., Andreae, M.O., Cantrell, W., Cass, G.R., Chung, C.E., Clarke, A.D., Coakley, J.A., Collins, W.D., Conant, W.C., Dulac, F., Heintzenberg, J., Heysfield, A.J., Holben, B., Howell, S., Hudson, J., Jayaraman, A., Kiehl, J.T., Krishnamurti, T.N., Lubin, D., McFarquhar, G., Novakov, T., Ogren, J.A., Podgorny, I.A., Prather, K., Priestley, K., Prospero, J.M., Quinn, P.K., Rajeev, K., Rasch, P., Rupert, S., Sadourny, R., Satheesh, S.K., Shaw, G.E., Sheridan, P., Valero, F.P.J., 2001. Indian Ocean Experiment: an integrated analysis of the climate forcing and effects of the great Indo-Asian haze. *J. Geophys. Res. Atmos.* 106, 28371–28398. <https://doi.org/10.1029/2001JD900133>.
- Rastogi, N., Singh, A., Singh, D., Sarin, M.M., 2014. Chemical characteristics of PM_{2.5} at a source region of biomass burning emissions: evidence for secondary aerosol formation. *Environ. Pollut.* 184, 563–569. <https://doi.org/10.1016/j.envpol.2013.09.037>.
- Reutter, P., Su, H., Trentmann, J., Simmel, M., Rose, D., Gunthe, S.S., Wernli, H., Andreae, M.O., Pöschl, U., 2009. Aerosol- and updraft-limited regimes of cloud droplet formation: influence of particle number, size and hygroscopicity on the activation of cloud condensation nuclei (CCN). *Atmos. Chem. Phys.* 9, 7067–7080. <https://doi.org/10.5194/acp-9-7067-2009>.
- Roberts, G.C., Nenes, A., 2005. A continuous-flow streamwise thermal-gradient CCN chamber for atmospheric measurements. *Aerosol Sci. Technol.* 39, 206–221. <https://doi.org/10.1080/027868290913988>.
- Rodhe, H., Grandell, J., 1972. On the removal time of aerosol particles from the atmosphere by precipitation scavenging. *Tellus* 24, 442–454. <https://doi.org/10.3402/tellusa.v24i5.10658>.
- Rose, D., Gunthe, S.S., Mikhailov, E., Frank, G.P., Dusek, U., Andreae, M.O., Pöschl, U., 2008. Calibration and measurement uncertainties of a continuous-flow cloud condensation nuclei counter (DMT-CCNC): CCN activation of ammonium sulfate and sodium chloride aerosol particles in theory and experiment. *Atmos. Chem. Phys.* 8, 1153–1179. <https://doi.org/10.5194/acp-8-1153-2008>.
- Rosenfeld, D., Fischman, B., Zheng, Y., Goren, T., Giguzin, D., 2014. Combined satellite and radar retrievals of drop concentration and CCN at convective cloud base. *Geophys. Res. Lett.* 41, 3259–3265. <https://doi.org/10.1002/2014GL059453>.
- Roy, A., Chatterjee, A., Sarkar, C., Das, S.K., Ghosh, S.K., Raha, S., 2017. A study on aerosol-cloud condensation nuclei (CCN) activation over eastern Himalaya in India. *Atmos. Res.* 189, 69–81. <https://doi.org/10.1016/j.atmosres.2017.01.015>.
- Sahai, S., Sharma, C., Singh, S.K., Gupta, P.K., 2011. Assessment of trace gases, carbon and nitrogen emissions from field burning of agricultural residues in India. *Nutrient Cycl. Agroecosyst.* 89, 143–157. <https://doi.org/10.1007/s10705-010-9384-2>.
- Sánchez, M., Longo, K.M., Freire, J.L.M., Freitas, S.R., Martin, S.T., 2017. Impact of mixing state and hygroscopicity on CCN activity of biomass burning aerosol in Amazonia. *Atmos. Chem. Phys.* 17, 2373–2392. <https://doi.org/10.5194/acp-17-2373-2017>.
- Sarangi, T., Naja, M., Ojha, N., Kumar, R., Lal, S., Venkataramani, S., Kumar, A., Sagor, R., Chandola, H.C., 2014. First simultaneous measurements of ozone, CO, and NO_y at a high-altitude regional representative site in the central Himalayas. *J. Geophys. Res. Atmos.* 119, 1592–1611. <https://doi.org/10.1002/2013JD020631>.
- Seibert, P., Kromp-Kolb, H., Baltensperger, U., Jost, D.T., Schwikowski, M., Kasper, A., Puxbaum, H., 1994. Trajectory analysis of aerosol measurements at high alpine sites. In: Borrell, P.M., Borrell, P., Cvetas, T., Seiler, W. (Eds.), *Proc. of EUROTRAC Symposium '94*. Academic Publishing BV, The Hague, Garmisch-Partenkirchen, Germany, pp. 689–693.
- Seinfeld, J.H., Pandis, S.N., Noone, K., 1998. Atmospheric chemistry and Physics: from air pollution to climate change. *Phys. Today* 51, 88–90. <https://doi.org/10.1063/1.882420>.
- Shrestha, P., Barros, A.P., Khlystov, A., 2010. Chemical composition and aerosol size distribution of the middle mountain range in the Nepal Himalayas during the 2009 pre-monsoon season. *Atmos. Chem. Phys.* 10, 11605–11621. <https://doi.org/10.5194/acp-10-11605-2010>.
- Siingh, D., Gopalakrishnan, V., Gautam, A.S., Singh, R.P., 2011. Estimation of aerosol size distribution from ion mobility spectra using the KL model. *Int. J. Rem. Sens.* 32, 6783–6798. <https://doi.org/10.1080/01431161.2010.512945>.
- Singh, A., Rajput, P., Sharma, D., Sarin, M.M., Singh, D., 2014. Black carbon and elemental carbon from postharvest agricultural-waste burning emissions in the Indo-Gangetic plain. *Adv. Meteorol.* <https://doi.org/10.1155/2014/179301>.
- Singh, R.P., Dey, S., Tripathi, S.N., Tare, V., Holben, B., 2004. Variability of aerosol parameters over Kanpur, northern India. *J. Geophys. Res. Atmos.* 109, 1–14. <https://doi.org/10.1029/2004JD004966>.

- Singla, V., Mukherjee, S., Kashikar, A.S., Safai, P.D., Pandithurai, G., 2019. Black carbon: source apportionment and its implications on CCN activity over a rural region in Western Ghats, India. *Environ. Sci. Pollut. Res.* 26, 7071–7081. <https://doi.org/10.1007/s11356-019-04162-w>.
- Srivastava, A.K., Tiwari, S., Devara, P.C.S., Bisht, D.S., Srivastava, M.K., Tripathi, S.N., Goloub, P., Holben, B.N., 2011. Pre-monsoon aerosol characteristics over the Indo-Gangetic Basin: implications to climatic impact. *Ann. Geophys.* 29, 789–804. <https://doi.org/10.5194/angeo-29-789-2011>.
- Stein, A.F., Draxler, R.R., Rolph, G.D., Stunder, B.J.B., Cohen, M.D., Ngan, F., 2015. NOAA's HYSPLIT atmospheric transport and dispersion modeling System. *Bull. Am. Meteorol. Soc.* 96, 2059–2077. <https://doi.org/10.1175/BAMS-D-14-00110.1>.
- Tang, M., Chan, C.K., Li, Y.J., Su, H., Ma, Q., Wu, Z., Zhang, G., Wang, Z., Ge, M., Hu, M., He, H., Wang, X., 2019. A review of experimental techniques for aerosol hygroscopicity studies. *Atmos. Chem. Phys.* 19, 12631–12686. <https://doi.org/10.5194/acp-19-12631-2019>.
- Tripathi, S.N., Dey, S., Tare, V., Satheesh, S.K., Lal, S., Venkataramani, S., 2005. Enhanced layer of black carbon in a north Indian industrial city. *Geophys. Res. Lett.* 32 <https://doi.org/10.1029/2005GL022564>.
- Upadhyay, R.G., Ranjan, R., Negi, P.S., 2015. Climatic variability and trend at Ranichauri (Uttarakhand). *J. Agrometeorol.* 17, 241–243.
- Usery, E.L., Varanka, D., Finn, M.P., 2009. Mapping developments and gis in the Usgs , 1884-2009. In: *Proc. 24th Int. Cartogr. Conf. Santiago Chile, Chile*.
- Wang, Y., Zhuang, G., Tang, A., Yuan, H., Sun, Y., Chen, S., Zheng, A., 2005. The ion chemistry and the source of PM_{2.5} aerosol in Beijing. *Atmos. Environ.* 39, 3771–3784. <https://doi.org/10.1016/j.atmosenv.2005.03.013>.
- Xue, L.K., Wang, T., Guo, H., Blake, D.R., Tang, J., Zhang, X.C., Saunders, S.M., Wang, W. X., 2013. Sources and photochemistry of volatile organic compounds in the remote atmosphere of western China: results from the Mt. Waliguan Observatory. *Atmos. Chem. Phys.* 13, 8551–8567. <https://doi.org/10.5194/acp-13-8551-2013>.
- Yarragunta, Y., Srivastava, S., Mitra, D., Chandola, H.C., 2020. Influence of forest fire episodes on the distribution of gaseous air pollutants over Uttarakhand, India. *GIScience Remote Sens.* 57, 190–206. <https://doi.org/10.1080/15481603.2020.1712100>.
- Zhang, Q., Jimenez, J.L., Canagaratna, M.R., Allan, J.D., Coe, H., Ulbrich, I., Alfarra, M. R., Takami, A., Middlebrook, A.M., Sun, Y.L., Dzepina, K., Dunlea, E., Docherty, K., DeCarlo, P.F., Salcedo, D., Onasch, T., Jayne, J.T., Miyoshi, T., Shimojo, A., Hatakeyama, S., Takegawa, N., Kondo, Y., Schneider, J., Drewnick, F., Borrmann, S., Weimer, S., Demerjian, K., Williams, P., Bower, K., Bahreini, R., Cottrell, L., Griffin, R.J., Rautiainen, J., Sun, J.Y., Zhang, Y.M., Worsnop, D.R., 2007. Ubiquity and dominance of oxygenated species in organic aerosols in anthropogenically-influenced Northern Hemisphere midlatitudes. *Geophys. Res. Lett.* 34 <https://doi.org/10.1029/2007GL029979>.
- Twomey, S. (1977). The Influence of Pollution on the Shortwave Albedo of Clouds, *Journal of Atmospheric Sciences*, 34(7), 1149-1152. [doi.org/10.1175/1520-0469\(1977\)034<1149:TPOPOT>2.0.CO;2](https://doi.org/10.1175/1520-0469(1977)034<1149:TPOPOT>2.0.CO;2).